AN EXTENDED TRAVELLING FIRE METHOD (ETFM) FRAMEWORK FOR PERFORMANCE-BASED STRUCTURAL DESIGN

Xu Dai*[1], Stephen Welch[1], Olivier Vassart[2], Kamila Cábová[3], Liming Jiang[4], Jamie Maclean[1], G. Charles Clifton[5], and Asif Usmani[4]

[1]School of Engineering, BRE Centre for Fire Safety Engineering, Institute for Infrastructure and Environment, The University of Edinburgh, Edinburgh, EH9 3FB, UK
[2]ArcelorMittal Steligence, 66 rue de Luxembourg, L-4009 Esch sur Alzette, Luxembourg
[3]Department of Steel and Timber Structures, Faculty of Civil Engineering, Czech Technical University in Prague, Thákurova 2077/7, Czech Republic
[4]Department of Building Services Engineering, The Hong Kong Polytechnic University, Hong Kong 999077, HK
[5]Department of Civil & Environmental Engineering, University of Auckland, Auckland, 1142, New Zealand

Abstract

This paper presents the extended travelling fire method (ETFM) framework, which considers both energy and mass conservation for the fire design of large compartments. To identify its capabilities and limitations, the framework is demonstrated in representing the travelling fire scenario in the Veselí Travelling Fire Test. The comparison between the framework and the test is achieved through performing a numerical investigation of the thermal response of the structural elements. The framework provides good characterisation of maximum steel temperatures and the relative timing of thermal response curves along the travelling fire trajectory, though it does not currently address a non-uniform fire spread rate. The test conditions are then generalised for parametric studies which are used to quantify the impact of other design parameters, including member emissivity, convective heat transfer coefficient, total/radiative heat loss fractions, fire spread rate, fire load density and various compartment opening dimension parameters. Within the constraints of this study, the inverse opening factor and total heat loss prove to be the most critical parameters for structural fire design.

Keywords

travelling fires; performance-based design; structural fire engineering; numerical heat transfer; Veselí Travelling Fire Test; large compartment fire

1 Introduction

In structural fire design, a key principle is to ensure that the fire resistance of a structure, assessed using some performance criteria, can handle expected fire severities. Short cuts can be taken in environments where the standard heating curve, e.g. ASTM-E119 fire[1], may be adopted as a reasonable surrogate for actual fire conditions (acknowledging the different assumptions for example via time equivalence), though under many real fire scenarios the discrepancy with the standard test must be explicitly addressed. At another extreme, considering large spaces with certain fire load distributions, such as car parks, localised fires, e.g. Hasemi localised fire model[2], may be invoked. In the large domain in between these limits, the simplifying assumptions of uniform or localised fire would be undermined, thus rendering assessment of structural fire performance much more challenging.

1.1 Why travelling fires

A classic example of the challenge of the large compartment fire problem is the World Trade Center (WTC) buildings collapse in New York City in 2001, for which fire is regarded as the prime reason[3]. The National Institute of Standards and Technology (NIST) reconstructed the potential fire impact inside of the building compartments using the Fire Dynamics Simulator (FDS) code, to further investigate the mechanisms leading to collapse of the buildings. They concluded that resort to compartment temperature averaging may lead to significant errors in the thermal and structural response, since the fire conditions were probably highly variable spatially, and moreover the main burning zone was observed to "travel" around the large compartment[4], as shown in Figure 1.

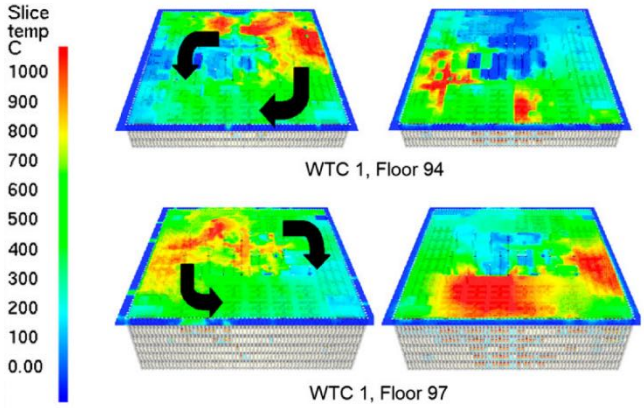

Figure 1. FDS simulated fire movement on floors 94 and 97 of WTC 1, adapted from Gann *et al.*[4].

Apart from the WTC buildings, high levels of temperature inhomogeneity in the large compartments with such developing/spreading fire features has been reported on many other occasions: the First Interstate Bank Building in Los Angeles in 1988[5], the Windsor Tower in Madrid in 2005[6], and more recently the Plasco Building in Tehran in 2017[7,8]. Furthermore, experimental evidence from dedicated tests has also shown a high degree of temperature heterogeneity in such compartments and the corresponding threat to the structures, with relevant experiments reviewed by Stern-Gottfried & Rein in 2012[9], and Dai *et al.* in 2017[10]. These facts underline the urgent need for a better description of fire scenarios for structural design, recognising the trend towards the larger spatial layouts often preferred in contemporary architecture. One possible solution is by performing Computational Fluid Dynamics (CFD) simulations[11–17], which can be used to derive the fire severity input for structural design. However, using CFD is typically not feasible on a day-to-day routine design basis for structural engineers, due to the massive computational demands and expert analyst effort it would entail. Moreover, the very detailed outputs that CFD models generate are necessarily tied to very specific and probably unrealistic definitions of the fire source and will typically embed excessive amounts of detail, which may be unwarranted for the purposes of defining sufficient thermal boundary conditions, and may even be misleading. Professional fire science knowledge is also needed to interpret and judge results derived from complex fire scenarios. In addition, outputs may often be highly sensitive to uncertain input parameters. An alternative solution, as proposed here, is to represent these types of fire scenarios by means of a simple design framework, which has been developed to address the problem in a practical manner, thereby enabling the structural engineers to utilise a general fire-structure coupling concept without resorting to excessively large computations. An appropriate level of detail in the model is required in order to represent the relevant fire scenarios in an efficient and realistic manner. The work in this paper is developed on this basis.

1.2 Travelling fire methodologies

In recent years, the problem described above has been addressed with so called 'travelling fire' methodologies, which relate to fires that are assumed to burn "locally" but which are presumed to move across entire floor plates over a period of time. There are three explicit representations of travelling fires which can be found in the literature: Clifton's model (1996)[18], Rein's model and its subsequent

refined versions (2007 onwards)[19–22], and an extended travelling fire methodology (ETFM) framework *conceptually* put forward by the authors in 2016[23,24]. The latter ETFM framework is postulated on a 'mobilised' version of Hasemi's localized fire model[2] for the fire plume near the structure (i.e. near-field), combined with a simple smoke layer calculation which utilises the FIRM zone model[25] for the areas of the compartment away from the fire (i.e. far-field). The temperature field generated by the ETFM framework will enable both a heating phase and a cooling phase for each structural member in the large compartment, schematically presented in Figure 2.

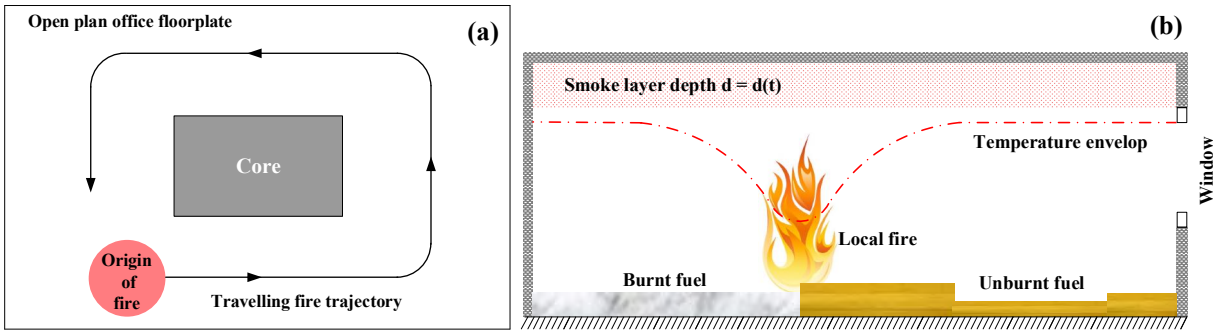

Figure 2. Schematic of the ETFM framework (a) in sectional plan view and (b) in sectional elevation view, adapted from Dai *et al.*[23].

The ETFM framework thereby enables the analysis to capture both spatial and temporal changes of the thermal field. Fire temperatures are variable for the near field, contrasting the uniform 800°C - 1200°C assumption in Rein's model, while all elements in one firecell are constrained to share the same fire exposure history in Clifton's model. Furthermore, the embedded FIRM zone model also enables the ETFM to consider smoke accumulation under the ceiling, which is not explicitly addressed in the other models. Significantly, by incorporating the FIRM zone model into the ETFM framework, both the energy and mass conservation are required to be satisfied for the design compartment. It is noted that previously proposed travelling fire methodologies have simply forced a travelling fire representation via specifying that the temperature field from other existing models will move through the compartment (i.e. modified parametric fire curves in Clifton's model, and the 800°C – 1200°C temperature block with Alpert's ceiling jet model in Rein's model), and have not attempted to explicitly account for the mass and energy balance in the compartment, thus the ETFM framework in principle addresses more of the fire dynamics. The work presented in this paper puts forward a performance-based design approach which is relatively easy to implement for structures with large compartments under travelling fires, through a more fire science-bounded travelling fire model which incorporates mass and energy conservation, i.e. the ETFM framework.

1.3 The openings for a design compartment

After more than a decade of research, travelling fires are now regarded as a very relevant fire scenario for large compartments. Typical features of this fire scenario are the fire plume in the near-field and the hot smoke layer which provides pre-heating in the far field. Once the fire is "travelling", the near-field has a leading edge representing the fire spread, and a trailing edge representing the burnout of the fuel. Though well understood in concept, the main research efforts on travelling fire methodologies[10] inevitably rely highly on an oversimplified assumption – that travelling fires are mostly fuel-load-driven, i.e. where ventilation plays a very limited role in dictating design fires in large compartments.

In literature, fuel load control is recognised not to hold for small fully engulfed compartments, in which inverse opening factor is one of the dominant variables affecting the maximum average gas-phase temperature[26,27], as shown in Figure 3. A value of the inverse opening factor of approximately 10 $m^{-1/2}$ separates the compartment fire regimes between "fuel-controlled" and "ventilation-controlled", and the maximum temperature decreases in both directions as the inverse opening factor deviates from this value. More recently, Torero *et al.*[28] revisited the conventional compartment fire framework, which is highly relevant to Figure 3 and developed by the pioneers in fire safety engineering (i.e. Kawagoe K., Thomas P.H., and Harmathy T.Z.), concluding that there is in fact no theoretical linkage between the

inverse opening factor and the maximum steady state temperature in the compartment for fuel-controlled fires, as historical experimental data shows a high degree of scatter between these two variables. However, they emphasized that the development of the conventional compartment fire framework was generally based upon roughly cubic compartments of relatively small size (< 150 m^3).

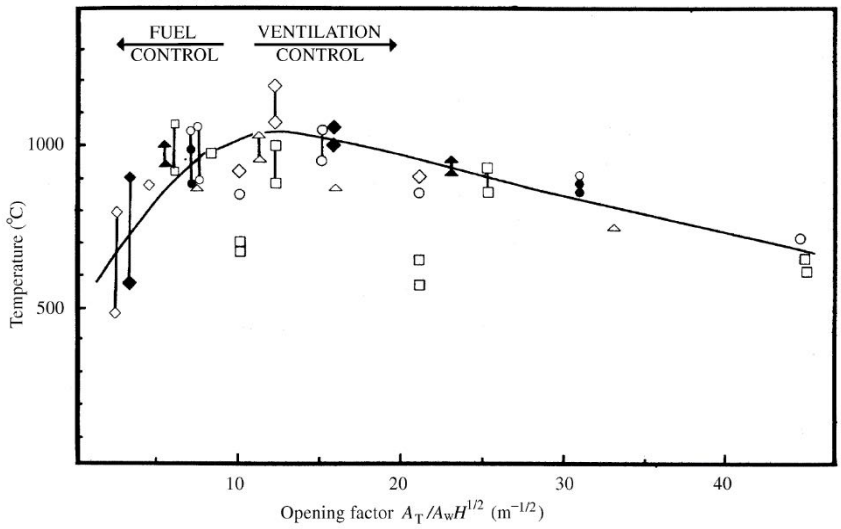

Figure 3. The relationship between the inverse opening factor $A_T/(A_wH^{1/2})$ and the maximum average gas-phase temperature in small size compartments, with smallest dimension of 0.5, 1 or 1.5 m (A_T is the total area of enclosure excluding floor and openings area, A_W is the total area of the vertical openings, and H is the weighted average of window heights)[26], extracted from Thomas & Heselden[27] (NB – the axis label is retained as "Opening factor" as used by the original authors).

Majdalani *et al.*[29] further explored both the ventilation-controlled and fuel-controlled fires experimentally and numerically, with a 0.82 m wide, 0.82 m high, and 1.06 m deep test compartment. Via extrapolation from these results it was suggested that fuel-controlled fires are more practical and perhaps more critical for structural fire design in large compartments, compared with ventilation-controlled fires. Via a test series in large compartments (5 m wide, 2 m high, and 18 m deep) Maluk *et al.*[30] quantitatively challenged the validity of the conventional compartment fire framework, through analysing the energy distribution under different ventilation conditions[31]. This analysis showed that the largest contribution to the energy loss is through compartment openings. This finding implies that considering fuel-controlled fires with large openings in a design compartment would generally underestimate the fire impact for structural design compared to ventilation control, and thus highlights the importance of addressing the role of the openings, and uncertainties in glazing failure, for a large design compartment under travelling fires. This implication is consistent with the observation and analysis of the NIST report for the First Interstate Bank Building fire[5], which was a high-rise building fire occurring in 1988 in Los Angeles, US, with large open-plan office areas (approx. 1394 m^2 on each floor). The fire started at the south-east corner of the 12th floor, and spread both horizontally and vertically to the upper floors (13th - 15th floors and part of the 16th floor), lasting for about two hours. It was noted that both the fire damage level and spread rate on the 12th floor were higher at the fire initiation area when the ventilation was limited, compared with the opposite side of the building on the 12th floor when the ventilation was improved due to the increasing number of window breakages as the fire developed and propagated.

Figure 4 compares the results of previous full-scale natural fire tests carried out in large compartments, where a clear travelling fire development had been identified or targeted, in order to investigate the relationship between the inverse opening factor $A_T/(A_wH^{1/2})$ and the maximum average gas-phase temperature $T_{g,max}$ near the ceiling level. The full-scale travelling fire experiments considered include: the British Steel Technical (BST)/Fire Research Station (FRS) 1993 fire test series[32], the Building Research Establishment (BRE) tests in the Cardington Large Building Test Facility (LBTF) in 1995-1996 (Test 6, Simulated Office)[33,34], the Moinuddin & Thomas fire test series[35] in 2005, the Veselí Travelling Fire Test[12] in 2011, the Edinburgh Tall Building Fire Tests (ETFT)[31,36] (tests number 11 and 12, using wood sticks) in 2013, the Malveira Fire Test[37,38] in 2014, the Tisova Fire Test[39] in 2015, and

the TRAFIR-RISE Fire Test in 2018. The detailed test set-up of these travelling fire experiments has been reviewed by the authors in a previous work[10], except for the Malveira Fire Test and TRAFIR-RISE Fire Test which were so far unpublished. There is no data point for another very relevant travelling fire test, the St. Lawrence Burns Project[40], as there is limited access to the detailed test data. It is important to note that the research target of the relevant tests was essentially the same, i.e. open-plan office buildings under natural fires. Hence, the fire load densities of those tests fall in a fairly close range, i.e. 40 - 46 kg/m^2 for wood cribs (except for the Malveira Fire Test for which 23 kg/m^2 was adopted), and methylated spirits in the Moinuddin & Thomas fire test series which generated broadly comparable heat release rates per unit area.

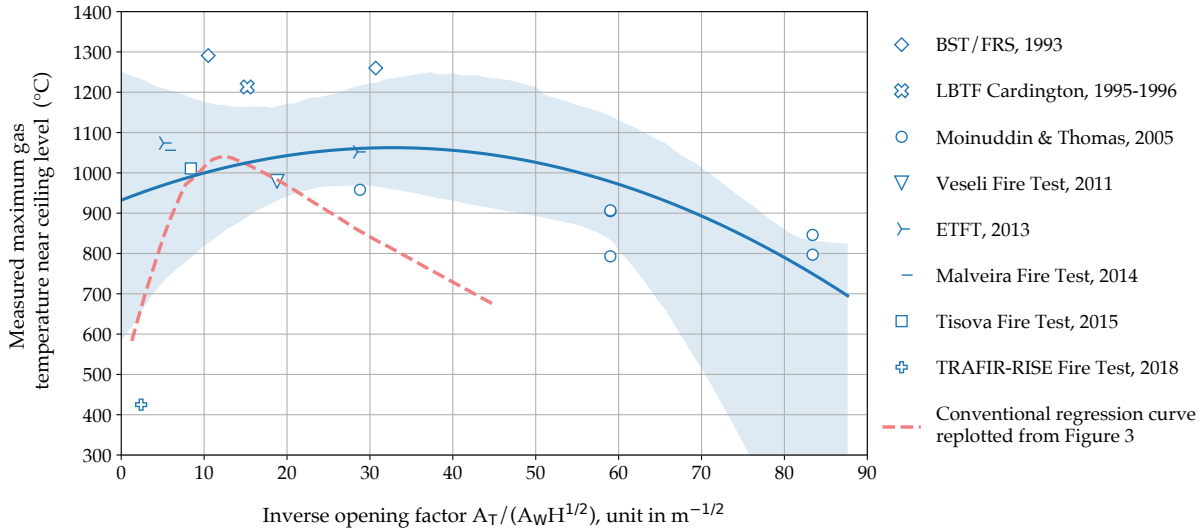

Figure 4. The relationship between the inverse opening factor $A_T/(A_w H^{1/2})$ and the measured maximum average gas-phase temperature $T_{g,max}$ near ceiling level of test large compartments. (solid curve in blue is the 2nd order polynomial regression line for all the reviewed travelling fire tests, and dashed red curve is the same curve presented in Figure 3 for small size compartments as a reference; the translucent blue band describes a bootstrap confidence interval of the estimated regression line according to the available data sampling points).

In general, Figure 4 illustrates that conditions in the majority of the travelling fire tests for large compartments lie in the traditional ventilation-controlled regime (i.e. the inverse opening factor is greater than 10 m$^{-1/2}$). However, the regression curve presented in Figure 4 suggests that the regime 'division number' might have shifted from about 10 m$^{-1/2}$ for small compartments to closer to 30 m$^{-1/2}$ for the large compartments reviewed here. Also, Majdalani *et al.*[29] have independently quantified the "break point" between regimes as being close to an inverse opening factor of 23.9 m$^{-1/2}$. When the inverse opening factor is larger than 30 m$^{-1/2}$, it is apparent that $T_{g,max}$ decreases when the inverse opening factor increases (i.e. smaller openings are adopted) in the large design compartment. This trend is supported by results from the single test series due to Moinuddin & Thomas 2005, which systematically explored a range of inverse opening factors. The main reason for this trend is apparent when considering that, in ventilation-controlled fires, as the opening size decreases, oxygen starvation may take place, thereby affecting the combustion efficiency and tending to reduce the average gas-phase compartment temperature. On the other hand, the relationship between the inverse opening factor and the $T_{g,max}$ is not very clear for the travelling fire tests with inverse opening factors less than 30 m$^{-1/2}$, let alone less than 10 m$^{-1/2}$. It only shows a weak dependence of the relationship, suggesting that the $T_{g,max}$ gradually decreases as the inverse opening factor is reduced. This dependence of the relationship is much less obvious compared with that for the small-size compartments under the fuel-controlled regime, as indicated by the left hand descending branch of the dashed red curve in Figure 4.

Based upon the above discussions, especially for the observations from the First Interstate Bank Building fire[5], the energy distribution analysis by Maluk *et al.*[30], and the regression curve for identifying the relationship between the inverse opening factor and $T_{g,max}$ from large scale travelling fire experiments (in Figure 4), it is apparent that the opening conditions for a design large compartment might still be a relevant design parameter in the travelling fire methodologies for performance-based structural design.

1.4 Research objectives

An extended travelling fire method (ETFM) framework is presented considering both the energy conservation and mass conservation for the design large compartment, for the purpose of assessing whether the structure is able to resist more realistic fire exposures expected in such compartments, for performance-based structural design. Some of the initial ETFM applications were presented in Dai *et al*. (2017)[10]. It is worth noting that those parametric studies were performed by running the 'travelling Hasemi' component and FIRM zone model component *separately*, to investigate the individual, rather than combined, thermal impacts.

The aims of the current work are to (1) present the full version of the ETFM framework with relevant design instructions which can be readily used by the structural fire engineers; (2) apply the ETFM framework to represent a travelling fire scenario in a real building, i.e. the Veselí Travelling Fire Test building, to further assess the capabilities and limitations of the framework; and (3) perform design parameter sensitivity studies, and parametric studies on the ETFM framework, for the same Veselí Test Building case, in order to interpret the importance of different design parameters (e.g. the inverse opening factor) for travelling fires.

2 ETFM Framework

The ETFM framework is developed by 'mobilising' Hasemi's localized fire model[2] for the fire plume near the structure (i.e. near-field). Further, since the Hasemi's equation is applicable to localized fires in an unconfined space and smoke accumulation is not considered in his model, this may lead to the far field predicted heat fluxes based on Hasemi's model being lower than the actual exposures in a confined space (though Hasemi's model is only applicable for the near-field). Therefore, Hasemi's model is combined with a hot smoke layer calculation (i.e. the FIRM zone model), which inherently enables the ETFM framework to consider both the energy and mass conservation for the design in a large compartment. It is then assumed that the radiant and convective heat fluxes to structural surfaces can be calculated based on the *summation* of heat flux from Hasemi's localized fire model and the heat flux from the FIRM zone model (see Figure 5). This might be conservative in the overlap zone. More importantly, it is worth noting that the ETFM in nature is a *framework*, i.e. the users could choose to replace Hasemi's model with other localised fire models, or FIRM with other zone models, depending upon the fire models' applicability in their specific design fire conditions.

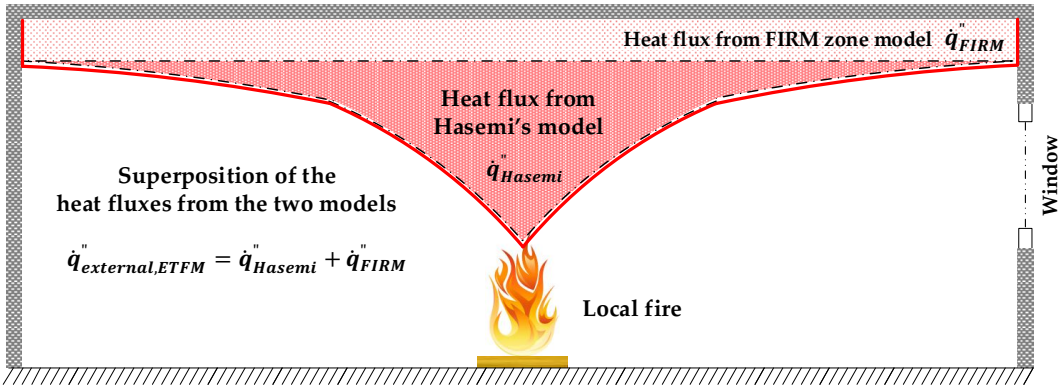

Figure 5. Heat fluxes 'combination' of the two models, i.e. Hasemi localised fire and FIRM zone model.

2.1 Near field: Hasemi's localized fire model

For quantifying the local effect of the travelling fire on adjacent structural members, Hasemi's localized fire model[2] is utilized in the ETFM framework. This correlation model was originally developed with a series of laboratory scale fire tests[41–44] in Japan, with maximum heat release rate (HRR) up to 900 kW. Later, additional model validation tests were conducted in Europe with fire size ranging from 2 MW to 60 MW, for both large compartments and car parks[45]. Franssen *et al*.[46] put forward three correlation equations which provide the external heat flux received at the level of the ceiling. These correlations

were eventually adopted in Eurocode 1 as the "localized fire model"[47]: when the fire plume is impinging the ceiling, the external heat flux, $\dot{h}$ (W/m^2), is given as:

$$\begin{aligned} \dot{h} &= 100000 && \text{if} && y \le 0.30 \\ \dot{h} &= 136300 - 121000y && \text{if} && 0.30 < y \le 1.0 \\ \dot{h} &= 15000y^{-3.7} && \text{if} && y \ge 1.0 \end{aligned} \tag{1}$$

The parameter y is obtained using the following equation:

$$y = \frac{r + H + z'}{L_h + H + z'} \tag{2}$$

where r (m) is the horizontal distance between the vertical axis of the fire and the point along the ceiling in which the heat flux is calculated, H (m) is the distance between the fire source and the ceiling, L_h (m) is the horizontal flame length (see Figure 6):

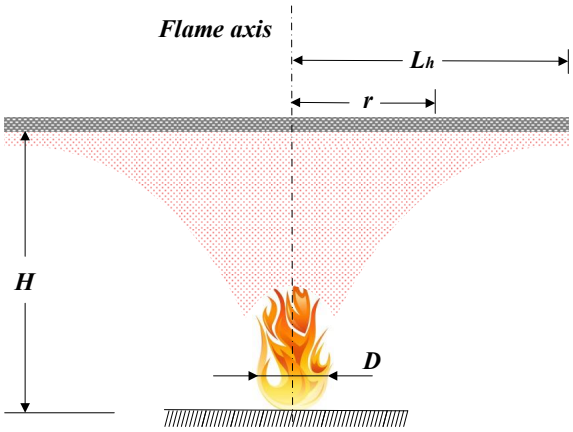

Figure 6. Hasemi's localized fire model, plot adapted from Eurocode 1[47].

L_h (m) is given by the following relation:

$$L_h = (2.9H(Q_H^*)^{0.33}) - H \tag{3}$$

with Q_H^* a non-dimensional HRR given by:

$$Q_H^* = \dot{Q}/(1.11 \times 10^6 \times H^{2.5}) \tag{4}$$

z' (m) is the vertical distance between the virtual fire origin and the fire source, which is given by:

$$\begin{aligned} z' &= 2.4D\left(Q_D^{*\,2/5} - Q_D^{*\,2/3}\right) && \text{if} && Q_D^* < 1.0 \\ z' &= 2.4D\left(1.0 - Q_D^{*\,2/5}\right) && \text{if} && Q_D^* \ge 1.0 \end{aligned} \tag{5}$$

where $Q_D^* = \dot{Q}/(1.11 \times 10^6 \times D^{2.5})$, D (m) is the diameter of the fire, $\dot{Q}$ (W) is the HRR of the localised fire. Hence, to employ Hasemi's localized fire model into the ETFM framework, three key parameters should be determined transiently: the location of the fire, the evolving fire diameter, D (m), and HRR, $\dot{Q}$ (W), because they are each constantly changing when fire 'travels' in the compartment. Details of how these parameters are approximated according to the features of the travelling fire are illustrated in the following several sections.

2.2 Far field: FIRM zone model

In most practical buildings, smoke will normally accumulate under the ceiling if its movement is

interrupted, due to the walls or smoke protection soffits which are built around the ceiling edges. This key idea of smoke accumulation is incorporated into the ETFM framework through utilising a zone model, in an elementary way. The depth of the smoke layer is taken to be time-dependent and uniformly distributed over the whole ceiling (as illustrated in Figure 7). This feature is therefore capable of reproducing the pre-heating and post-heating effects required for the structural design. There are several zone models available in the literature, with two popular ones being OZone[48,49] and CFAST[50]. However, the ETFM framework employs the FIRM zone model[25] for its smoke layer calculation. The main reason is that FIRM is relatively simple and easy to implement, which matches the ethos of the ETFM framework. At the same time FIRM possesses all the basic components that a zone model should have, i.e. fire source, smoke plume, air entrainment, hot upper layer, cold lower layer, smoke flow through vents, and heat losses through thermal boundaries (i.e. walls, ceilings), and the most fundamental: mass conservation and energy conservation. It was also the first fire model which was fully documented, validated, verified, and evaluated following the ASTM guidelines back in 2000[25,51].

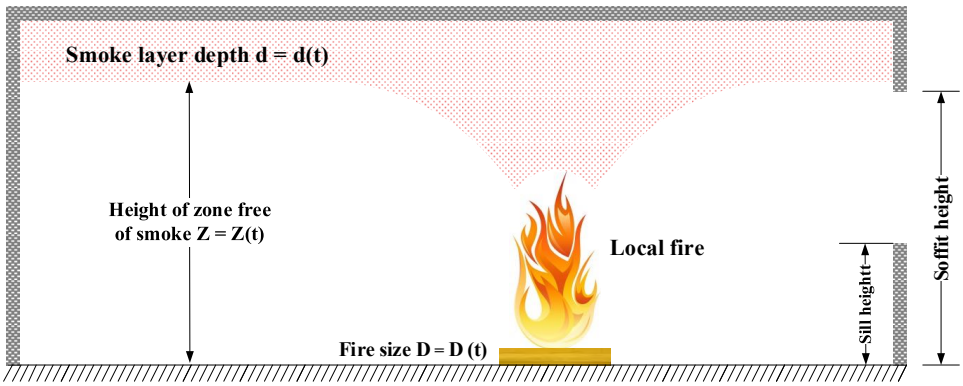

Figure 7. Schematic of the smoke for far field in the ETFM framework.

Two time-varying outputs are represented through the FIRM zone model, i.e. the transient upper smoke layer temperature, T_u (K), and the evolution of the smoke layer interface height, Z_i (m). The determination of these two variables is achieved via solving a set of ordinary differential equations (ODEs) based on mass and energy conservation, such as the mass conservation of the lower ambient air to obtain transient Z_i[25]:

$$\frac{dZ_i}{dt} = \frac{\dot{m}_a - \dot{m}_l - \dot{m}_e}{\rho_a A} \tag{6}$$

where t (s) is the time, $\dot{m}_a$ (kg/s) is the vent flow rate of the ambient air entering the compartment (an upper limit $(\dot{m}_a)_{max} = 0.52A_v\sqrt{H_v}$ is setup for ventilation-controlled burning while oxygen is limited, in which A_v is the area of the vertical opening, H_v is the clear opening height), $\dot{m}_l$ (kg/s) is the lower layer vent flow rate leaving the compartment, $\dot{m}_e$ (kg/s) is the air entrainment mass flow rate, $\rho_a = 1.2$ kg/m^3 is the density of the ambient air, and A (m^2) is the total compartment area, see Figure 8.

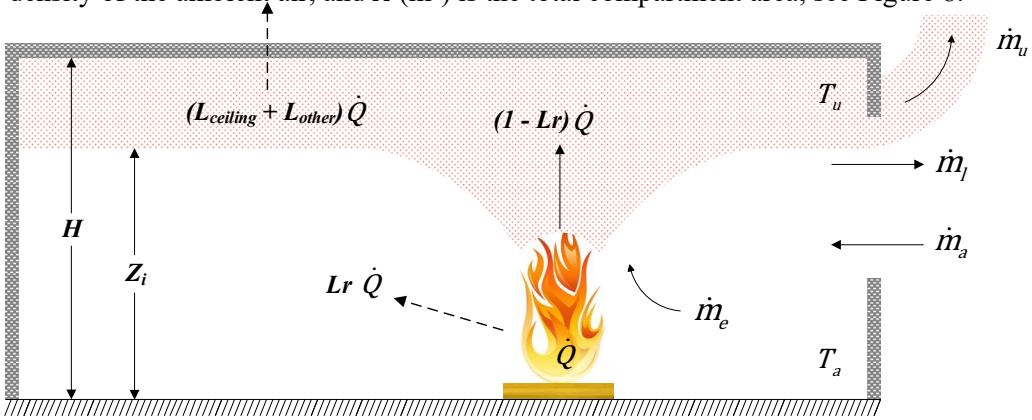

Figure 8. Schematic of the mass conservation and energy conservation of the FIRM zone model in ETFM.

Figure 8 schematically illustrates the mass and energy balance of the design compartment. In addition to the mass balance in this figure, $\dot{m}_u$ (kg/s) is the smoke vent flow rate leaving the compartment, and

H (m) is the clear height of the compartment. Another key ODE concerns the upper smoke layer energy conservation which is used to obtain the transient upper layer temperature, T_u[25]:

$$\frac{dT_u}{dt} = \frac{T_u\left[(1-L_c)\dot{Q} - \dot{m}_e c_p (T_u - T_a)\right]}{c_p \rho_a T_a A (H - Z_i)} \tag{7}$$

where $\dot{Q}$ (kW) is the HRR of the fire, $T_a = 294.26$ K is the ambient air temperature, $c_p = 1.004$ kJ/kg·K is the assumed constant specific heat, and L_c is the assumed constant total heat loss fraction ratio (0.6 ~ 0.9 as recommended in Janssens[25], in general, 0.6 refers to well-insulated compartment thermal boundaries while 0.9 refers to poorly-insulated compartment thermal boundaries).

In addition, L_r is the radiative loss fraction of the fire plume (0.15 ~ 0.40 as recommended in Janssens[25]). The relationship between L_c and L_r is explained in Eqn. 8, where the total heat loss fraction L_c consists of $L_{ceiling}$ (the fraction of heat losses in the form of ceiling convection), L_r, and L_{other} (heat losses fraction due to the roughness of ceilings or aspect ratio of the compartment, suggested to vary from 0 for very smooth ceilings or high aspect ratio compartments, to 0.3 for very rough ceilings or low aspect ratio compartments[25]).

$$L_c = L_r + L_{ceiling} + L_{other} \tag{8}$$

In the ETFM framework, only L_c and L_r need to be specified, hence $L_{ceiling} + L_{other}$ can be obtained as a lumped value. It is worth noting that L_c and L_r are both empirical values but they are very fundamental to the resultant smoke layer temperature calculations. Figure 8 also schematically illustrates the energy balance of the design compartment. Typically, a part of the total HRR of fire, $L_r\dot{Q}$, is assumed to be radiated away from the combustion region, and the rest $(1-L_r)\dot{Q}$ is convected up through the plume into the formation of the upper hot smoke layer. A fraction of this energy $(L_{ceiling} + L_{other})\dot{Q}$ is assumed to be lost from the smoke layer to the compartment boundaries through convection and radiation. Then the remaining energy at the upper layer, $(1-L_c)\dot{Q}$, would directly contribute to the gas temperature of the smoke, i.e. the sensible enthalpy. It is important to note that another main source of energy loss is through the openings. This is accounted for by the format of mass loss from the hot smoke layer venting, and explicitly calculated by the mass balance calculation for the entire compartment, which is given as:

$$\dot{m}_u T_u - \dot{m}_e (T_u - T_a) - \rho_a T_a A \frac{H - Z_i}{T_u}\frac{dT_u}{dt} + (\dot{m}_a - \dot{m}_l) T_a = 0 \tag{9}$$

It is anticipated there may be no significant differences in terms of smoke temperature rises by using different air entrainment models[52], nevertheless, two are made available in the ETFM framework: the Thomas model[53], which is widely used in the UK for venting calculations[26]:

$$\dot{m}_e = 0.188 W_{fi} (Z_i)^{3/2} \tag{10}$$

where W_{fi} (m) is the perimeter of the fire, and Zukoski's model[54], which is given as:

$$\dot{m}_e = K(1-L_r)^{1/3} \dot{Q}^{1/3} (\Delta Z_i)^{5/3} \tag{11}$$

where $K = 0.076$, ΔZ_i is the distance between the fuel top surface and the smoke layer interface. In the ETFM framework, the thickness of the fuel is ignored, hence $\Delta Z_i = Z_i$.

2.3 Heat release rate (HRR) $\dot{Q}$

The two critical important parameters in the ETFM framework are the travelling fire speed, which determines how long the "mobile" Hasemi localized fire will affect the structural element involved in the localised burning; and its total HRR, $\dot{Q}$, which determines how efficiently the thermal energy will

be released due to the fire plume. The total HRR, $\dot{Q}$, discussed in this section is to be used for Eqns. 4 and 5 to implement Hasemi's localized fire model, and Eqns. 7 and 11 to implement the FIRM zone model, both transiently. Although in Eurocode 1 the expression for calculating HRR, $\dot{Q}$, during the fire growth phase (t-squared fire evolution) is specified[47], the development phase of the travelling localized fire is not considered to be significant from the structural design point of view. Due to this reason, and for retaining the simplicity of the ETFM framework, the total HRR, $\dot{Q}$(W), is given by the following expression according to Eurocode 1:

$$\dot{Q} = 1000 \times RHR_f \times A_{fi} \tag{12}$$

where A_{fi} (m^2) is the burning area of the fuel, RHR_f (kW/m^2) is the maximum HRR per unit area. The determination of RHR_f for different occupancies can be referred to Eurocode 1[47] (250 kW/m^2 and 500 kW/m^2 are commonly used). Since RHR_f is a value corresponding to the 'stationary' state of the fire, it implies that the fire in the ETFM framework is actually a "localised fully engulfed" fire which covers a certain burning area of the fuel (i.e. A_{fi}), and travels along the floor plate as time evolves. Furthermore, the entrainment-controlled burning is considered in FIRM[25], which means the upper bound values are assumed for the air mass flow rate, $\dot{m}_e$, and corresponding HRR, $\dot{Q}$. Assuming Zukoski's plume model, $\dot{m}_e$ and $\dot{Q}$ are changed to:

$$(\dot{m}_e)_{max} = 55K^{3/2}(1 - L_r)^{1/2}(\Delta Z_i)^{5/2} \tag{13}$$

$$(\dot{Q})_{max} = 3030(\dot{m}_e)_{max} \tag{14}$$

As this ETFM framework is basically a localized fire travelling along a predefined trajectory, i.e. one-dimensional, the burning area of fuel A_{fi} is determined by three variables: the travelling fire *leading* edge derived from the assumed constant fire spread rate, v (mm/s), the travelling fire *trailing* edge derived from the burn-out time, t_b (s), and the compartment width derived from the floor plan dimensions. Figure 9 illustrates how the burning area of fuel, A_{fi} (m^2), is obtained, schematically.

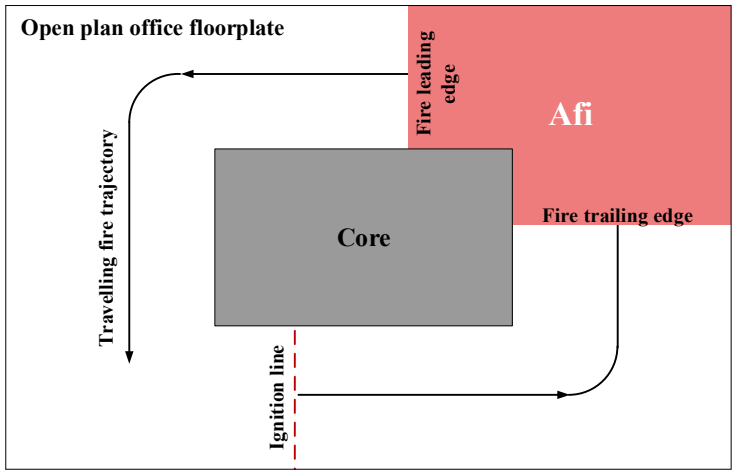

Figure 9. The determination of burning area of fuel A_{fi}.

2.4 Speed of the travelling fire

Fire spread rates will vary hugely depending on the circumstances, thus for design exercises a range will normally be specified; in defining representative numbers some have analysed real fires, Rackauskaite *et al.*[22] and Dai *et al.*[10] citing numbers in the range 0.1-20 mm/s. Clifton[18] adopted rates of 8.3 mm/s for low opening factors (<0.06) and twice that for higher ones. Franssen *et al.*[55] reported fire spread rates range from 0.6 mm/s to 7 mm/s in their experimental test series.

2.5 Burn-out time t_b

In this ETFM framework it is assumed that all fuel would be consumed over the entire fire duration. Therefore, to determine the travelling fire trailing edge location, a burn-out time, t_b (s), is introduced. t_b is a similar variable assumed in Rein's travelling fire model[22] for quantifying the time needed for burning out a certain area of fuel completely. It is obtained by the following equation:

$$t_b = 1000 \times q_{f,k}/RHR_f \quad (15)$$

where $q_{f,k}$ (MJ/m^2) is the characteristic fuel load density (depending on different occupancies, with a range of 100 to 1500 MJ/m^2 cited in Eurocode 1[47]). Figure 10 schematically illustrates how the burning area of fuel A_{fi} is determined with the burn-out time t_b concept.

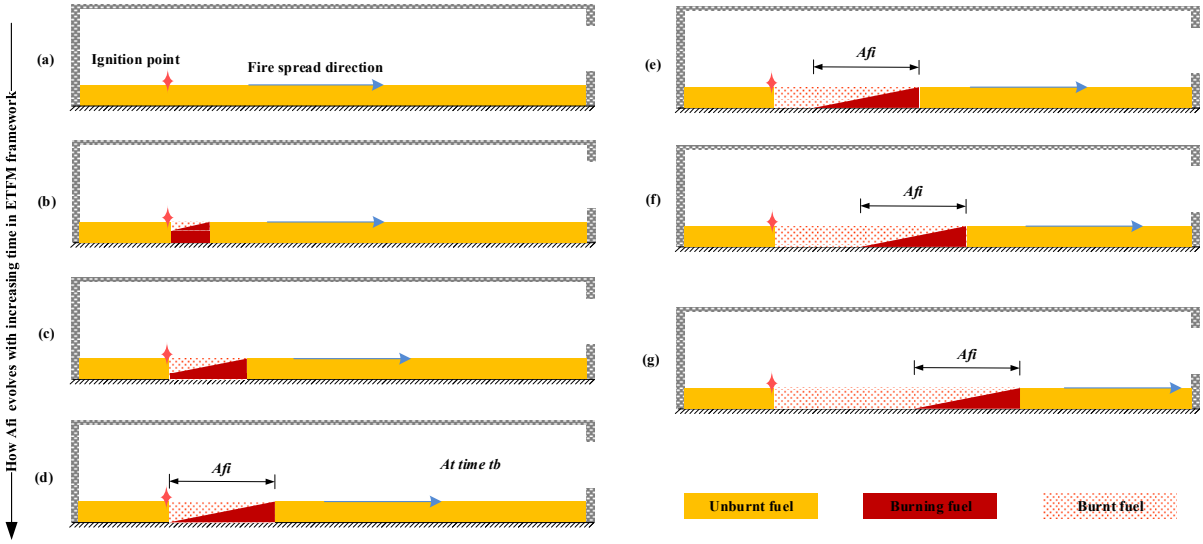

Figure 10. Determination of burning area A_{fi} with burn-out time t_b concept – in elevation view, (a) to (g) with a certain time sequence.

2.6 Approximation of Fire Location and Fire Diameter *D*

Once the burning area of fuel A_{fi} is determined, the fire location of the travelling Hasemi's localized fire model can be obtained, which is defined as the centre of the distance between the travelling fire leading edge and trailing edge along the trajectory. Furthermore, the fire diameter D (m) of the travelling Hasemi's localized fire can be approximated as the diameter of a circular source of the same burning area of fuel A_{fi} (m^2), which is given by Eqn. 16. It is worth nothing that Hasemi's localized fire model is only applicable for fire diameters less than 10m in the Eurocode[47].

$$D = 2\sqrt{A_{fi}/\pi} \quad (16)$$

2.7 Other key assumptions

As the final objective of this ETFM framework is for application to structural design, the travelling fire trajectory is assumed to be under the mid-span of the main beams (see Figure 2(a)), which would normally represent the worst case for the structural response. A concept of "regulatory minimum fuel depth" (RMFD) is introduced into the ETFM framework, corresponding to a reference travelling fire spread rate, v, and a certain level of fuel load density, $q_{f,k}$. This RMFD is a layer of fuel uniformly distributed over the entire floor plate, and contributes to the total heat flux calculation. The unburnt fuel in Figure 10 is an RMFD. The ETFM framework considers both the fuel-controlled and ventilation-controlled conditions, with the assumption that sufficient air is available at the beginning and subsequently the glazing adjacent to the main fire region breaks. This is likely to happen in many fires

considering window glazing failure at 150°C – 300°C[56]. Then the analysis may step into the entrainment-controlled burning or the ventilation-controlled burning, depending on the transient status of the air entrainment mass flow rate, $\dot{m}_e$, and the ambient air inflow rate through the compartment openings, $\dot{m}_a$, respectively. A flashover scenario arises naturally in this model, and the fire may transition from a localized travelling fire to flashover when a defined threshold is met, e.g. the temperature of the hot smoke layer reaches 600°C[26].

2.8 Implementation of the ETFM framework

To facilitate the ETFM framework as an easy-to-use design tool for the structural fire engineers, it is implemented into an OpenSees-based[57], open-source software framework called SIFBuilder[24,58–61] using C++. SIFBuilder integrates the analysis of fire, heat transfer and thermo-mechanical response of the structure in one single software package. The detailed implementation and verification of the ETFM framework is presented elsewhere[59]. SIFBuilder is used with the ETFM framework to perform both the fire and heat transfer analysis in the subsequent sections of this paper. Figure 11 schematically illustrates how the ETFM framework is implemented in a workflow manner, with referring to corresponding key subsection numbers, figures, and equations.

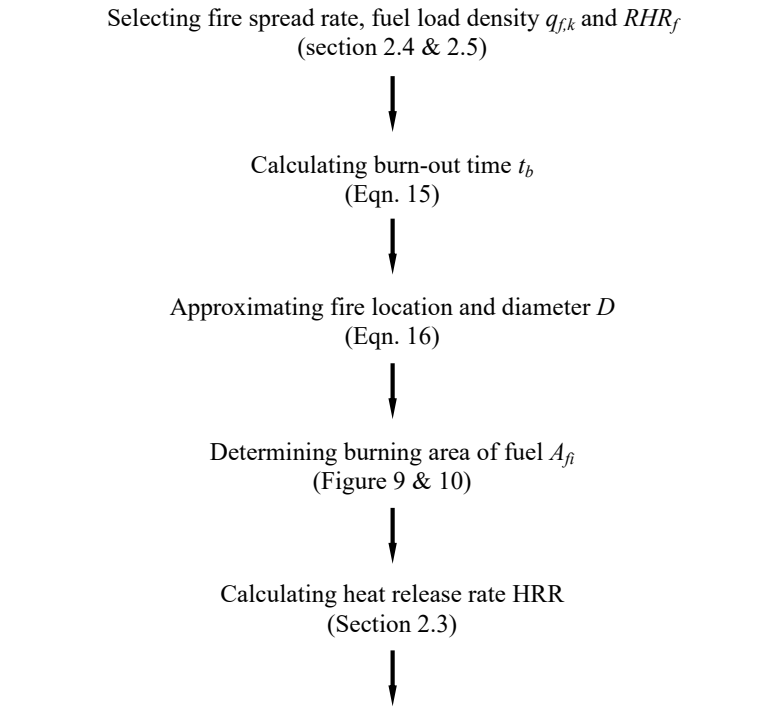

Figure 11. Flowchart - implementation of the ETFM framework.

3 Application of the ETFM Framework for the Veselí Travelling Fire Test Building

Performance-based design for structures in fire requires validated methodologies. Validation of fire spread predictions is very ambitious, nevertheless, in literature it is apparent that none of the travelling fire design methods have been rigorously compared against any real travelling fire experiments so far[10]. This section demonstrates the application of ETFM framework to representation of fire spread in a real building, i.e. the Veselí Travelling Fire Test building[12] (a two-storey steel-composite structure, as shown in Figure 12). It is achieved through performing a numerical investigation of the thermal response of the structural elements, i.e. comparing the computed member temperatures from the ETFM framework and the test results. The efforts of this comparison demonstrate the capability of the ETFM framework, as well as identifying some of its current limitations.

3.1 Veselí Travelling Fire Test (Czech Republic, 2011)

Figure 12. Experimental building during the Veselí Travelling Fire Test.

In 2001, a travelling fire test was conducted on the upper floor of a two-storey steel composite building in Veselí, Czech Republic, as part of a collaborative project funded by Research Fund for Coal and Steel (RFCS) in the European Commission, called COMPFIRE[62]. The test aimed to investigate how a travelling fire might impact the structural components, especially for beam-to-column connections[12].

The overall dimensions of the test building were 13.4 m long × 10.4 m wide × 9 m high, with a 5 m × 2 m unglazed opening on each floor to provide enough ventilation for a smooth development of the fire[63], as presented in Figure 13. The test compartment internal size was 12 m × 9 m, with 4 m in height. The test compartment was well-insulated[63], as linear trays K 120/600/0.75 mm + mineral wool Rockwool 120 mm in depth with density 40 kg/m^3 + trapezoidal sheet TR 35/207/0.63 mm were used as the wall linings, and 100 mm depth steel-composite slabs were used as the ceiling with lightweight concrete C30/37 + steel S350 trapezoidal sheets Cofraplus 60 with thickness 0.75 mm. The fuel bed was continuous in a 'band strip' shape (8 m × 3 m), using wood sticks (50 mm × 50 mm × 1000 mm per stick) as the fuel load. Every square metre of fuel bed consists of 6 layers of 7 wood sticks, approximately to fuel load density of 47.25 kg/m^2 (i.e. equivalent to 680 MJ/m^2 assuming a heat of combustion [64] of 18 MJ/kg, with combustion efficiency[65] 0.8), as shown in Figure 14.

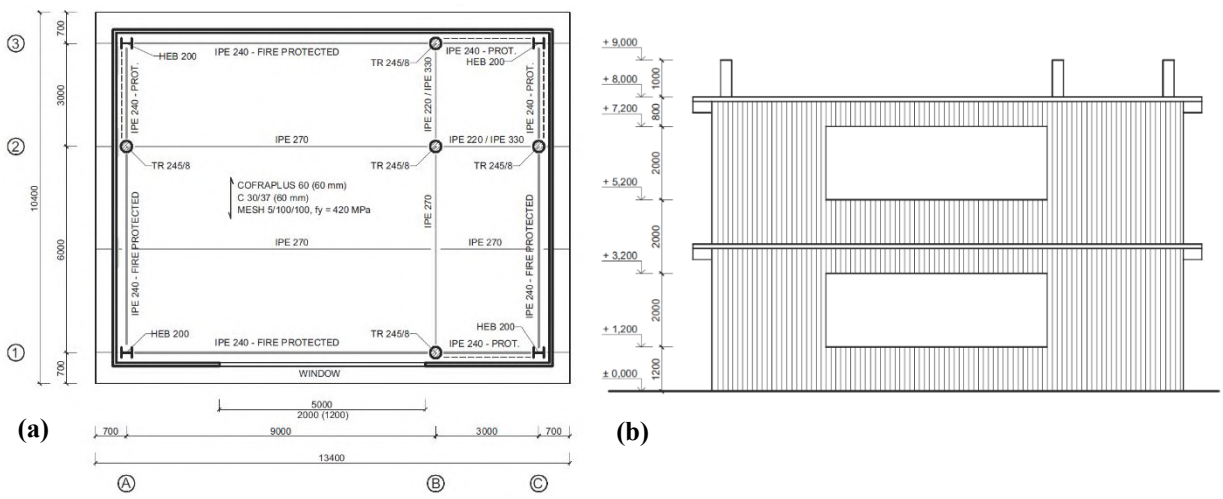

Figure 13. Veselí test building in (a) plan-view with approximate clear floor area 12 m × 9 m, and (b) in elevation view with one side vertical opening 5 m × 2 m on the test upper floor (dimensional unit in plots is mm), and 4 m in height, from Wald *et al.*[63].

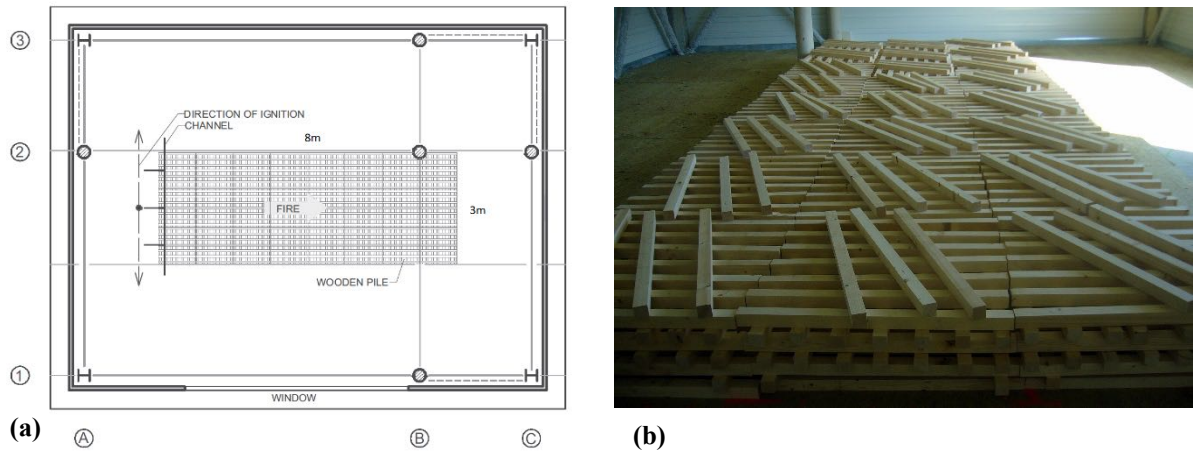

Figure 14. Veselí Travelling Fire Test fuel load scheme (a) in hatched 8 m × 3 m, on the upper floor of the experimental building[63], and (b) front view with wood stick size 50 mm × 50 mm × 1000 mm, with 6 layers of 7 sticks per square metre, approximate to fuel load density 680 MJ/m^2 within the hatched fuel bed.

Figure 15. Fire development in the Veselí Travelling Fire Test[10].

The fire was ignited with a linear source at one end of the fuel bed to allow it to develop along the length. Figure 15 demonstrates the fire development at every 5 mins during the test. Three phases can be identified: Phase I from 0 to 15 mins, while the fire leading edge was gradually spreading over the majority of the fuel bed and a clear smoke layer accumulation was observed; Phase II from 20 to 25 mins, while post-flashover conditions prevailed during this short time period, no external flames coming out of the opening were noted; Phase III from 25 to 40 mins, the fire trailing edge was progressing to the other end of the fuel bed, accompanied by a clear decaying of the fire. Thus, this travelling fire was partially fuel-controlled when the fire was spreading and decaying during Phase I and Phase III, and partially influenced by the ventilation when the smoke accumulation occurred during Phase I and post-flashover during Phase II.

Figure 16(a) presents the well-instrumented test compartment[63], including gas-phase temperature via thermocouple (TG series), plate thermometer temperature (PT series), radiant heat flux (R series), beam temperature (TB series), connection temperature, slab temperature (TS series), and column temperature (TSG series). Furthermore, unlike other travelling fire tests, the structural response during the fire development was also recorded, including the vertical and horizontal displacement of the slab (V and H series, respectively), the deflection of the beam mid-span (V series), and the strain gauge on the columns (SG series). Nevertheless, it is worth noting that the crib weight loss was not measured, which means it is not easy to characterise the evolving heat release of the fire.

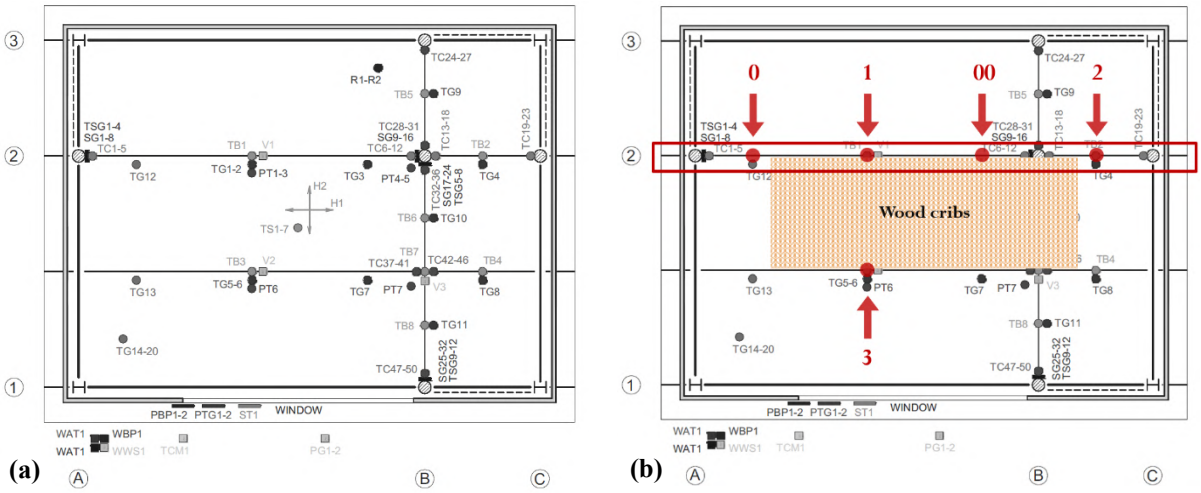

Figure 16. (a) Instrumentations at the test compartment ceiling level[63], details of these instrumentation symbols can be found in the main text, and (b) investigated TG and TB locations for the ETFM framework comparison with the test data (marked in red dots, with tags 0, 1, 00, 2, and 3, corresponding to TG12, TB1 & TG2, TG3, TB2 & TG4; and TB3 & TG6 respectively).

3.2 Heat transfer validation of SIFBuilder

In order to compare the thermo-mechanical representation of the ETFM framework with the Veselí Travelling Fire Test, locations near ceiling level (i.e. the bottom flange of the steel beams) with tags 0, 1, 00, 2 are selected for investigation, as shown in Figure 16(b). The reason for selecting this series of locations is because those points are arranged parallel with the travelling fire trajectory, and relatively far away from the openings, to minimise the wind-induced test data uncertainty. Furthermore, it is not straightforward to compare the heat flux from the ETFM framework with the measured thermocouple (TC) temperatures from the test, considering that the ETFM framework essentially generates heat fluxes as the thermal boundaries for the subsequent heat transfer analysis, and all four investigated locations 0, 1, 00, 2 have gas-phase temperature measurement via thermocouples at the vicinity of the lower flange of the steel beams (with corresponding tags TG12, TG2, TG3 and TG4, respectively). Alternatively, temperatures at the bottom flange of the steel beams may be chosen as the targeted variable for comparison, which requires heat transfer analysis using the heat flux from the ETFM framework, and TC temperatures from the test as the thermal boundaries, respectively.

SIFBuilder is used to perform the proposed heat transfer analysis for comparison. As mentioned in Section 2.8, it is an integrated numerical tool based on several OpenSees-related thermal modules, in which the heat transfer module was originally developed, and extensively verified as well as validated, by Jiang[66]. Nevertheless, the validity of applying the heat transfer module for the conditions of the Veselí Travelling Fire Test still needs to be quantified, and if it is necessary, the built-up heat transfer model may require to be further calibrated with the test data for the subsequent comparison. In addition, due to the limited number of measurement points (with bottom flange steel temperatures only TB1 at location 1 and TB2 at location 2, but TB1 failed after 15 mins during the test), another location with tag 3 (having measurements TB3 and TG6) is introduced as an additional heat transfer validation point, as shown in Figure 16(b).

Figure 17 shows an encouraging agreement between the measured steel beam bottom flange temperatures, TB2 and TB3, and the SIFBuilder heat transfer results, which use the corresponding lower flange TC temperatures in the vicinity, TG4 and TG6, respectively. The measured TG4 and TG6 are applied as the thermal boundaries on three sides of the investigated steel beam IPE270, excluding the top of the beam where a steel-composite slab is located. Two-dimensional heat transfer analysis is carried out for the cross-section, using the convection coefficient, $h_c = 35$ W/m^2 K as 'natural fire' for the fire-exposed surfaces, and emissivity of the steel, $\varepsilon_m = 0.7$ (two values as recommended in the

Eurocode[47]). Figure 17(a) shows that SIFBuilder heat transfer results at TB2 are slightly higher than the measured TB2, when the maximum temperature reaches to 782°C and 714°C, respectively. In addition, the SIFBuilder results at TB2 reach the maximum temperature about 3.6 mins later than the measurement. Moreover, Figure 17(b) demonstrates that the SIFBuilder heat transfer results at TB3 agree well with the measured TB3, in terms of the maximum temperatures, 727°C and 748°C, respectively. In this case, the timing is very close, i.e., reaching a peak at around 25 mins. It is important to note that there are large uncertainties here, because in reality both h_c and ε_m evolve according to the fire development and the steel beam heating process, respectively. A related uncertainty is the use of TC temperature which may depart from the local gas temperature which is strictly required as an input to convective heat transfer, but differences in the hot layer may be minor (Welch *et al.*[67]).

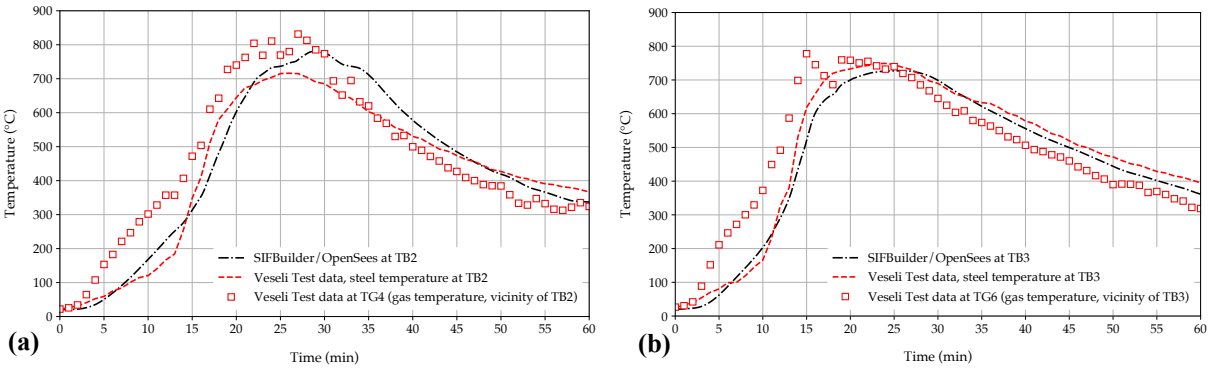

Figure 17. Heat transfer (HT) results from SIFBuilder at the bottom flange of the steel beams IPE270, at (a) TB2 at location 2 using TC temperature TG4 as HT input, and at (b) TB3 at location 3 using TC temperature TG6 as HT input, to compare the measured steel beam bottom flange temperatures with the SIFBuilder HT results.

3.3 ETFM framework vs. Veselí Travelling Fire Test

Figure 18(a) quantitatively confirms the three phases of fire development identified in section 3.1 during the test. At Phase I (0 - 15 mins), measured TC temperatures at locations 0, 1, 00 and 2 are all increasing due to the spreading of the fire leading edge. Meanwhile, a clear 'time difference' is also found among the four time-temperature curves, mainly due to the relative locations of those measured TCs along the fire trajectory. To be more specific, during the initial 5 mins the TC temperature histories at locations 0, 1 and 00 are very close to each other when the fire started, and TC temperature at location 2 is relatively lower, as it is far from the current burning fuel bed. From 5 to 15 mins the above trend is clearer, even among the TC temperature histories at locations 0, 1 and 00. At 15 mins, the results show that TG2 at location 1 reaches as high as 885°C, due to the direct fire exposure right beneath this location; TG12 at location 0 reaches 726°C, which is slightly higher than TG3 at location 00, which reaches 643°C, when the fire travels away from location 0 and into the direction of location 00. After the flashover transition from 15 to 20 mins, at Phase II (20 - 25 mins) all TCs reach their maximum temperatures, where TG2 and TG3 both reach around 950°C and TG12 and TG4 around 800°C. This maximum temperature difference between the centre of the compartment (location 1 and 00) and the edge of the compartment (location 0 and 2), again, challenges the conventional post-flashover compartment fire models with an assumed uniform temperature distribution (e.g. standard fire, or parametric fire curves). After 25 mins, including Phase III (30 - 40 mins), measured TC temperatures at locations 0, 1, 00 and 2 are all decreasing due to the movement of the fire trailing edge (i.e. the decay of the fire). This is different from Phase I where a clear 'time difference' was identified among those time-temperature curves as the fire spread along the fire trajectory; in contrast, all the time-temperature histories 'converge' to a very similar cooling trend here, from 30 mins to 60 mins. This suggests that the cooling stage is not mainly driven by the decaying of the burning fuel, as no 'time-difference' is identified, but is mainly due to the compartment characteristics, such as the thermal boundaries.

Figure 18(b) presents the heat transfer results from SIFBuilder at the bottom flange of the steel beams using the corresponding measured TC temperatures as heat transfer boundary conditions, at locations

0, 1, 00 and 2. Locations 0, 1 and 00 are at the vicinity of steel member IPE270, while location 2 is at vicinity of steel member IPE220, see Figure 13(a). The convection coefficient, $h_c = 35$ W/m^2 K and emissivity of the steel, $\varepsilon_m = 0.7$, are adopted, according to the work done in section 3.2. In addition, Figure 18(b) shows a very similar heating and cooling sequence among those four time-temperature histories at the bottom flanges, compared with what is presented in Figure 18(a).

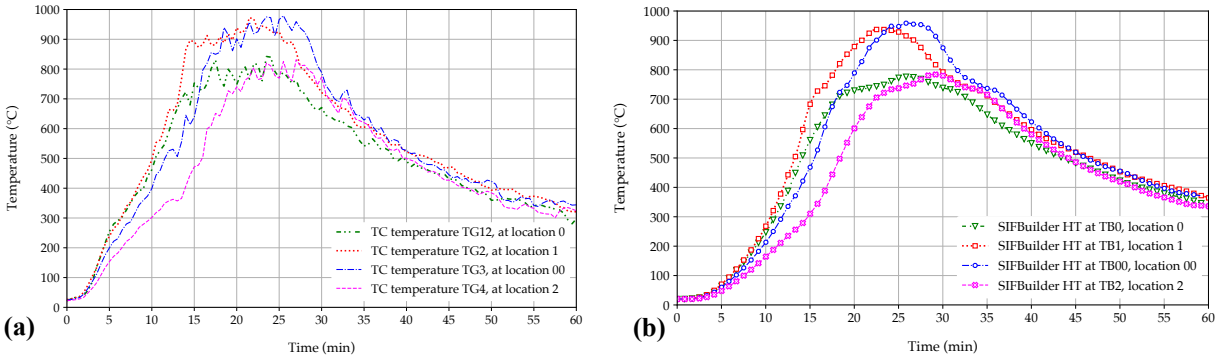

Figure 18. Temperature development along fire trajectory in the test at locations 0, 1, 00 and 2, through representing (a) measured thermocouple (TC) temperatures at the vicinity of the lower flange of the steel beams, and (b) heat transfer (HT) results from SIFBuilder at the bottom flange of the steel beams using the measured TC temperatures shown in (a) as HT input boundary conditions (same colours for curves in (a) & (b) if at corresponding same locations).

To achieve the comparison between the ETFM framework and the Veselí Travelling Fire Test, it is worth noting that the selected input parameters for the ETFM framework have three sources: 1) the exact test setup information, including compartment dimension 12 m × 9 m, fuel load distribution shape 8 m × 3 m, opening size 5 m × 2 m, opening location (i.e. sill height 1.2 m), and fire ignition location; 2) estimated values based on the relevant test publications, including total heat loss fraction 0.68 according to the thermal lining information from the test[63], fuel load density 680 MJ/m^2 with an assumed chemical heat of combustion of the wood sticks[64] to 18 MJ/kg with combustion efficiency[65] 0.8, fire spread rate 6.5 mm/s based on test observations, and maximum HRR per unit area according to Horová *et al.*[64]; 3) empirical values/formulas, e.g. Zukoski's plume model[54], and radiative heat loss fraction 0.25 as recommended in Janssens[25]. During the process of selecting appropriate parameters for the EFTM framework, it is important to clarify that, both source 2) and source 3) would introduce a certain level of modelling uncertainties. Such uncertainties are unavoidable, so it is of great importance to perform a certain level of fire modelling calibration with the test and subsequent parameter sensitivity studies, as suggested by Torero *et al.*[68], rather than to directly proceed to the "validation" of the fire model. Two parameters are adjusted for the calibration, i.e. the fire spread rate 6.5 mm/s, and the total heat loss fraction ratio 0.68. According to the test observation, the fire spread rate was accelerating throughout Phase I, see Figure 15. A rough estimate of the averaged fire spread is 3, 5.8 and 8.9 mm/s, corresponding to fire spreads up to positions at 0.9, 3.5 and 8 m, at 5, 10 and 15 mins, respectively. Due to the steady spread velocity assumption of the current version of ETFM framework, a constant value of 6.5mm/s is adopted. Subsequent to calibration using total heat loss fraction, $L_c = 0.68$, a reasonable comparison between the ETFM framework and the test is found. Though it will vary with time in practice, the value of $L_c = 0.68$ lies within the general range of $0.6 \sim 0.9$ as recommended by Janssens[25], where generally 0.6 refers to well-insulated compartment thermal boundaries, and 0.9 refers to poorly-insulated compartment thermal boundaries. In the test, 120mm mineral wool (Rockwool®) was used, which will therefore tend to be more towards the well-insulated condition.

Figure 19 demonstrates the comparison through quantifying beam member bottom flange temperatures at various locations along the fire trajectory, between the computed member temperatures using the ETFM framework and the calculated time-temperature histories using the test TC data as heat transfer input. A constant fire spread rate of 6.5 mm/s is used in the ETFM framework, in contrast to the accelerating fire spread of 3 to 8.9 mm/s observed in the test. In an attempt to correct for this offset all computed member temperatures from the framework presented in Figure 19 are shifted by 4 mins. It suggests a good agreement between the ETFM framework and the test in terms of maximum steel temperatures at various locations along the fire trajectory.

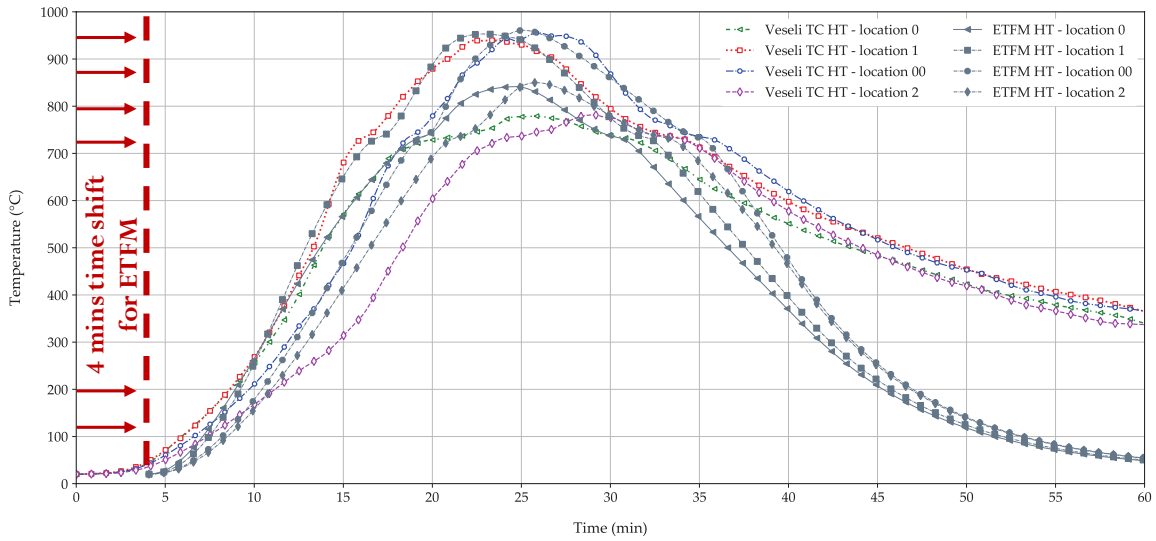

Figure 19. Comparison between the ETFM framework and the Veselí Test, using steel temperatures at bottom flanges, at locations 0, 1, 00 and 2 respectively in the fire spread direction (Veselí thermocouple (TC) temperatures at the vicinity of beam bottom flanges are used as input for SIFBuilder heat transfer).

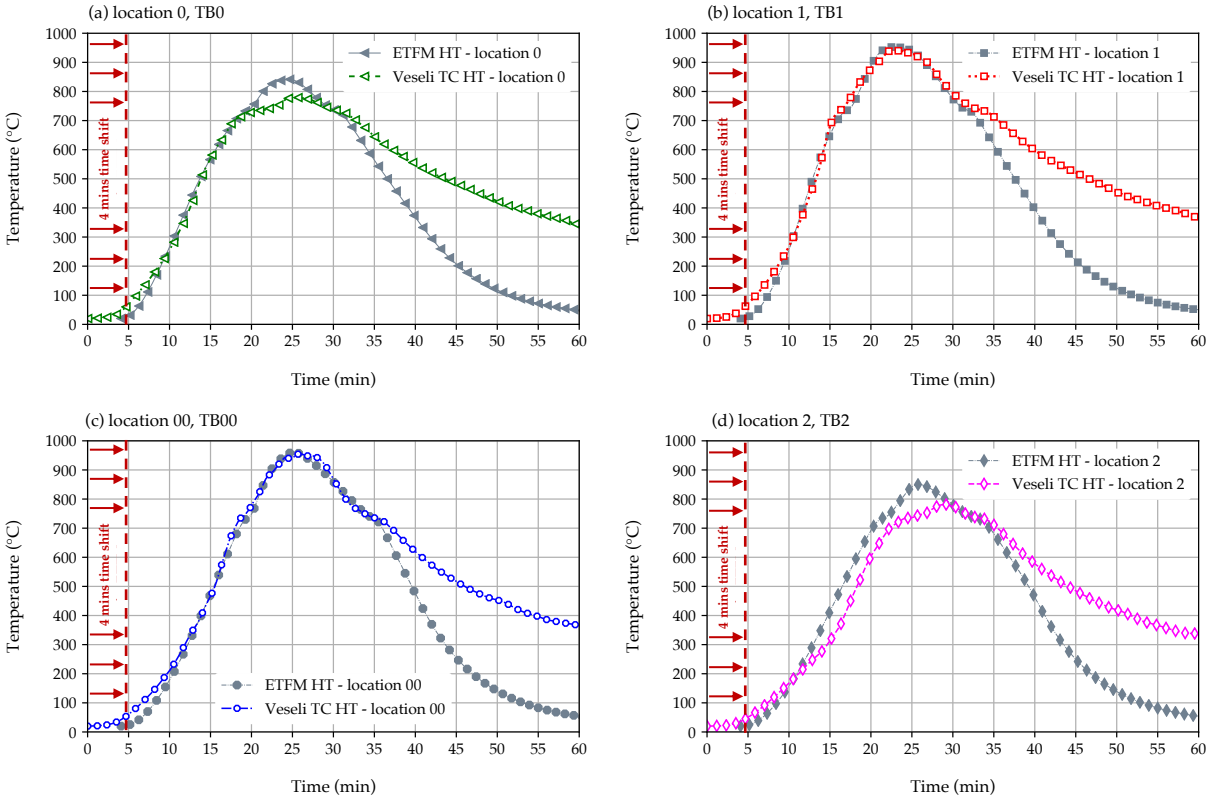

Figure 20. Comparison between the ETFM framework and the Veselí Test (with 4 mins time shift), using steel temperatures at bottom flanges, at various locations in the fire spread direction, (thermocouple (TC) temperatures at the vicinity of beam bottom flanges are used as input for SIFBuilder heat transfer), (a) location 0, (b) location 1, (c) location 00, and (d) location 2.

Figure 20 (a-d) presents the time-shifted comparison using the beam member bottom flange temperatures between the ETFM framework and the test at location 0, 1, 00 and 2, respectively. These four figures indicate that the ETFM framework can generate generally good reproductions during the heating stage of the travelling fire at various locations along the fire trajectory. The agreement is less good at location 2, which is at the opposite side of the fire ignition location. This suggests that the uniform temperature assumption due to the pre-heating of the smoke upper layer from the FIRM zone

model of the ETFM framework may over-predict the temperature in the far-field. However, this slight over-prediction is not of great concern, being conservative. More noticeably, a large discrepancy is found at all four locations during the decay stage. This is undesirable as it implies that the predicted time-temperatures from the ETFM framework may be far lower than the test results. A possible reason is that the ETFM framework links hot layer temperatures only to the fire HRR, whereas in the real case energy release and heat transfer continues from the glowing embers and the residual heat in the enclosure. Similar discrepancies were also identified when using a CFD model for the same test, by Horová *et al.*[12].

3.4 Parameter sensitivity studies on using ETFM framework for the Veselí Travelling Fire Test

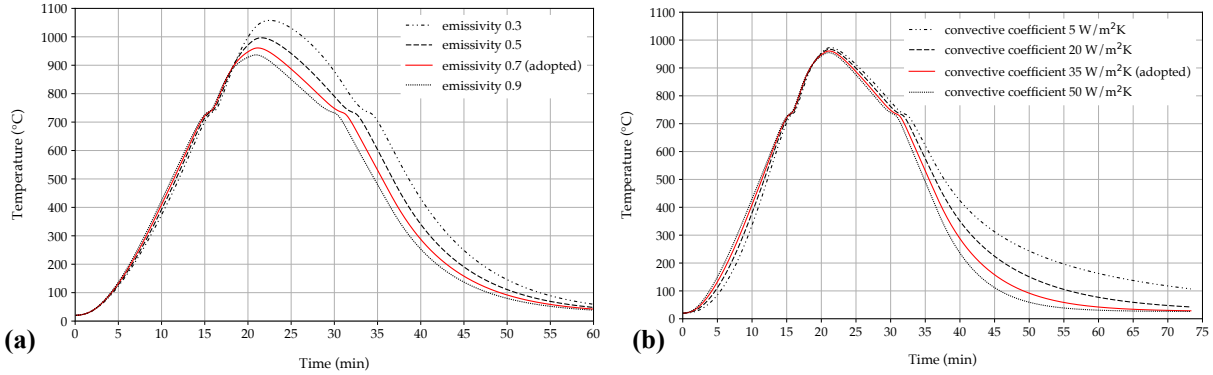

Figure 21. Steel beam bottom flange temperatures at location 00 using ETFM, with (a). various emissivity ε_m ranging from 0.3 to 0.9; (b). various convective coefficients h_c ranging from 5 W/m²K to 50 W/m²K.

For assessing the performance of the model, it is important to quantify the uncertainties of the input parameters, especially the steel emissivity, ε_m, convective coefficient, h_c, total heat loss fraction, L_c, and radiative heat loss fraction, L_r. Figure 21(a) shows that higher ε_m values would generate lower steel temperatures. Figure 21(b) shows the higher influence of h_c during the cooling phase of the travelling fire. Figure 22 suggests that both total heat loss fraction, L_c, and radiative heat loss fraction, L_r, dominate the maximum steel member temperatures. The uncertainties of the heat loss fraction parameters have fundamentally different origins: L_c is simply because of the complexity of the travelling fire processes, and in reality it is neither constant spatially or temporally, hence a lumped constant value was assumed in the FIRM zone model (see Eqns. 7 and 8), while L_r is a design parameter that is more related to the burning of fuel itself (see Janssens[25]). Nowadays, as buildings are tending to become more and more 'energy efficient', the energy loss may be more limited and lower L_c values may need to be considered in design solutions. The L_c value range is suggested in Janssens[25].

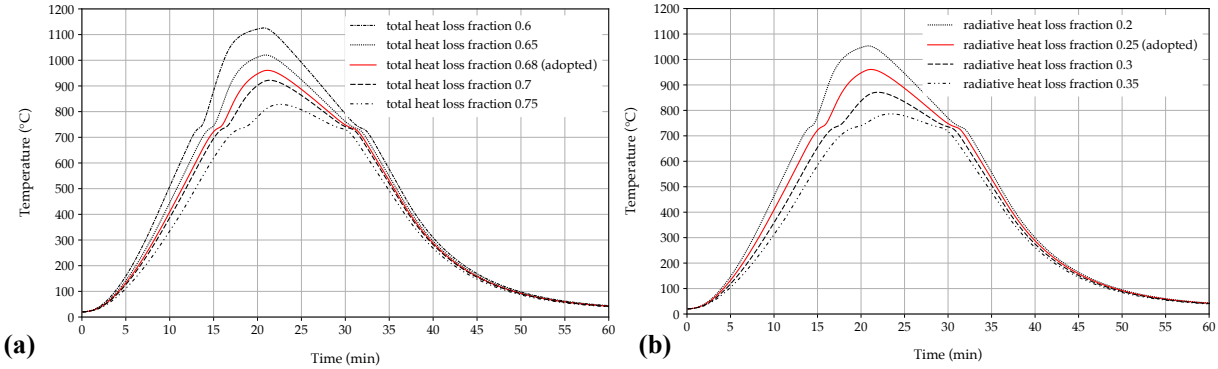

Figure 22. Steel beam bottom flange temperatures at location 00 using ETFM, with (a). various total heat loss fraction L_c ranging from 0.6 to 0.75; (b). various radiative heat loss fraction L_r ranging from 0.2 to 0.35.

4 Further Parametric Studies on using ETFM Framework for the Veselí Travelling Fire Test

When a structural engineer is to design a beam in a building, an assumed design load must be chosen. Hence, safety factors with specific building design loads are adopted in order to make sure the member has enough 'load bearing margin' under different possible loading combinations. However, in structural fire design, there is no exact methodology or procedure available, especially while defining design fires within very large compartments, for performance-based design. In such cases it is recommended that a series of design parametric analyses should be performed, through changing the design fire parameters, to generate a family of travelling fires to check the reliability of the design solutions (e.g. including the maximum steel member temperatures, and the time to reach such temperatures). This section provides an example of such analysis. Based on the same Veselí travelling fire test case, some of the design parameters are extended, e.g. various fuel load densities, opening dimensions, etc.

Figure 23(a) demonstrates that the travelling fire scenarios with higher fire spread rates, v (e.g. 8 mm/s, 9.5 mm/s) will generate higher temperatures and temperature increase rates. This is because of the more rapid growth in HRR (see Eqn. 12), which is manifest in higher layer temperatures, via the energy conservation equation from the FIRM zone model (see Eqn. 7). The 'faster' fires produce higher thermal impact due to bigger fire areas and higher temperatures (hence fluxes). For increased fuel load densities burning durations also increase, and the resulting higher fire temperatures also result in higher steel temperatures, as per Figure 23(b). The effect is compounded by that fact that they also have larger fire areas, thus producing higher thermal impacts.

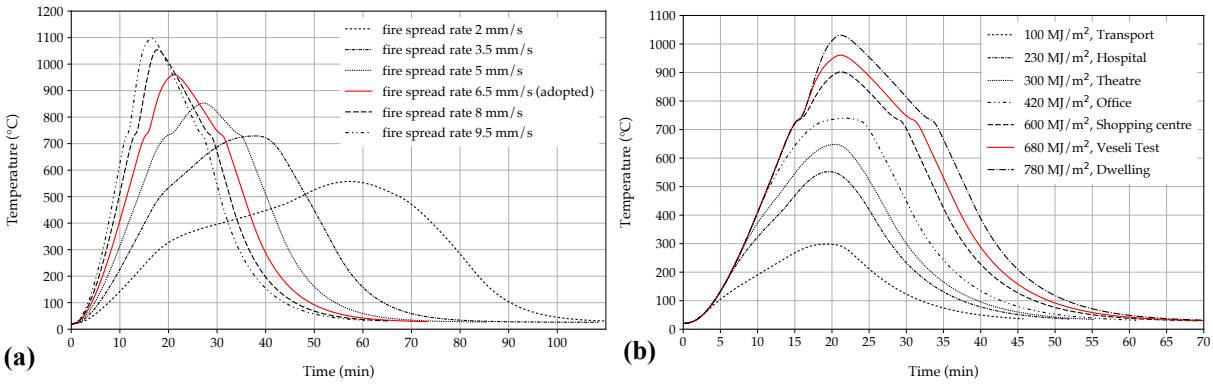

Figure 23. Steel beam bottom flange temperatures at location 00 using ETFM, with (a). various fire spread rates ranging from 2 mm/s to 9.5 mm/s, as suggested in Rackauskaite *et al.*[22]; (b). various fuel load densities ranging from 100 MJ/m² to 780 MJ/m², as suggested in Eurocode 1[47].

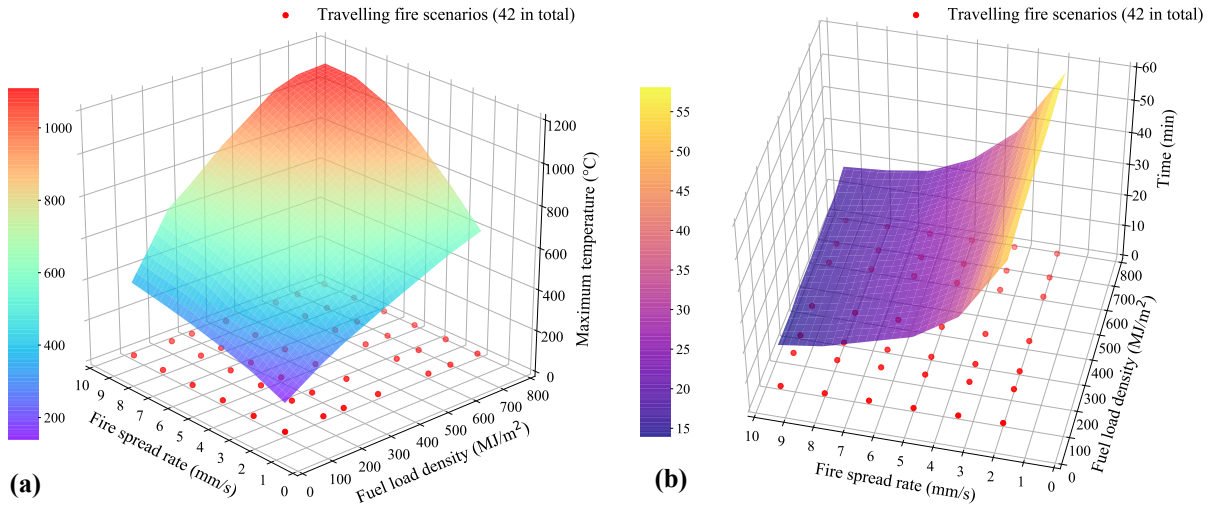

Figure 24. Various combinations of different fire spread rates (ranging from 2 mm/s to 9.5 mm/s) and fuel load densities (ranging from 100 MJ/m² to 780 MJ/m²) with 42 travelling fire scenarios, marked with red dots as sampling points, with (a). maximum steel beam bottom flange temperatures at location 00; (b). time to reach the peak temperature of the steel beam bottom flange at location 00.

Due to the computational efficiency of the ETFM framework in SIFBuilder a large set of travelling fire scenarios combining various fire spread rates v and fuel load densities $q_{f,k}$ can be analysed for very modest computational cost. Here, a parametric set of 42 cases is analysed, considering the same values of v and $q_{f,k}$ as adopted for Figure 23(a) and (b), respectively, and further illustrated with corresponding red dots in Figure 24(a) and (b). Figure 24(a) demonstrates the maximum bottom flange temperatures of the investigated steel beam at location 00, ranging from 139 to 1108°C. Higher maximum temperatures are captured with higher v and $q_{f,k}$, due to larger fire sizes and HRRs. Figure 24(a) implies v and $q_{f,k}$ are 'equally' influential on the resultant maximum temperatures, while for the travelling fire scenarios falling within the red ring (i.e. red: above 800°C). However, such 'equivalent influence' diminishes while the travelling fire scenarios progress into the 'green and blue ring' (i.e. green and blue: below 800°C). This green and blue ring changes its 'profile' compared with the red ring, implying that the fuel load density has a stronger impact than fire spread rate under such fire scenario combinations. Figure 24(b) shows the time to reach maximum temperature of the investigated steel beam at location 00, ranging from 14 to 58 mins. This figure suggests that the fire spread rate is a more discriminating factor rather than the fuel load density, i.e. in terms of affecting time to reach peak temperatures in the beam.

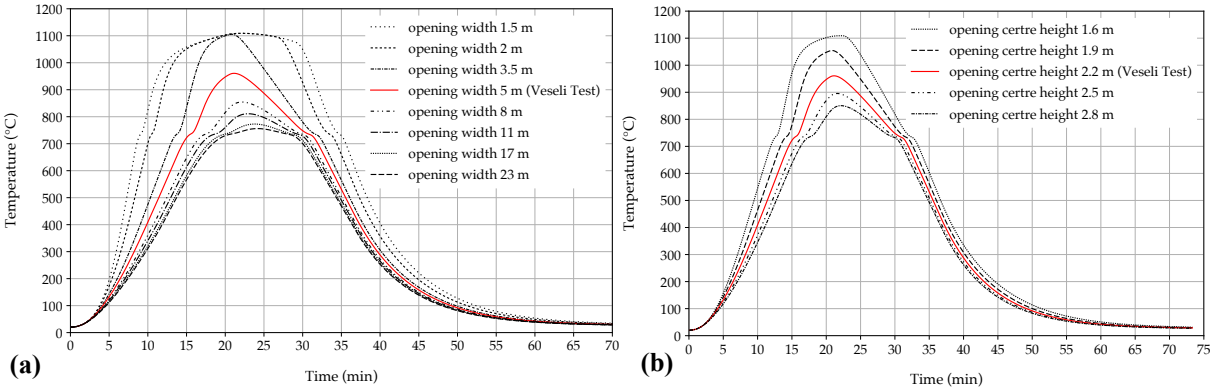

Figure 25. Steel beam bottom flange temperatures at location 00 using ETFM, with (a). various opening width W ranging from 1.5 m to 23 m; (b). various opening centre locations H_o, (sill height + soffit height)/2, ranging from 1.6 m to 2.8 m (opening dimension kept the same as the Veselí Travelling Fire Test Building, 5 m × 2 m).

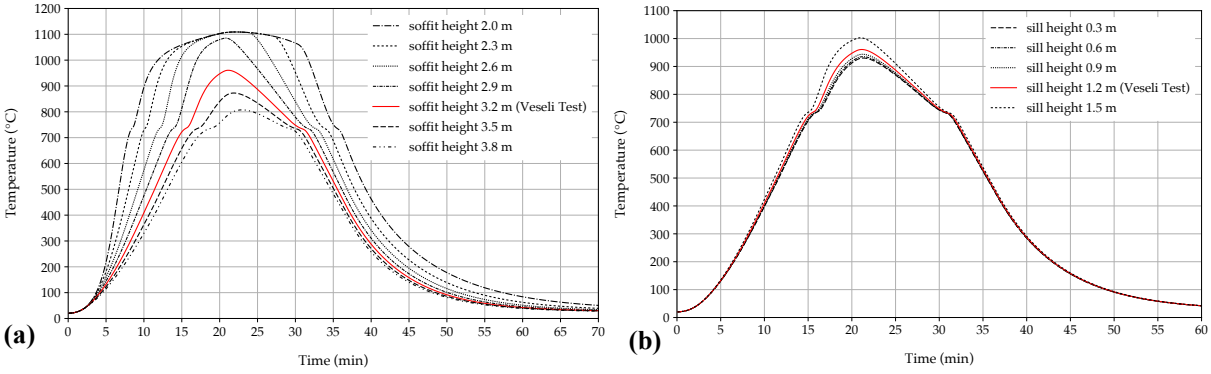

Figure 26. Steel beam bottom flange temperatures at location 00 using ETFM, with (a). various soffit heights ranging from 2.0 m to 3.8 m; (b). various sill heights ranging from 0.3 m to 1.5 m.

Figure 25(a) shows the impact of the opening width on the resultant steel member bottom flange time-temperature histories at location 00. All of the input parameters for this series of travelling fires are the same as the ones presented in Section 3.3, except for the variance of opening width. It suggests that smaller opening widths would yield higher steel temperatures and longer heating durations. The reason is probably that reducing the opening width will confine more upper smoke layer mass and energy within the compartment, i.e. less mass and energy from the hot upper layer is lost through the openings, as suggested by Eqns. 6 and 7. When the travelling fire scenarios have relatively small opening widths,

i.e. 1.5, 2 and 3.5 m, their maximum temperatures seem to coincide to an upper limit, at approximately 1106°C. The small opening sizes may constrain the ambient air inflow through the compartment cold layer, with $(\dot{m}_a)_{max} = 0.52A_v\sqrt{H_v}$ (see section 2.2) for ventilation-controlled burning, while oxygen is limited. Figure 25(a) further suggests that when the opening width increases, i.e. opening width is greater than 8 m in this Veselí case, that the dependence relationship between the maximum steel temperature and the opening width is less clear. Then, the maximum temperature of the steel member tends to be more related to the fuel load itself, rather than the openings. Figure 25(b) shows that the increase of the opening centre height would tend to decrease the steel member temperature, as the smoke hot layer neutral plane is 'moved upward', which thereby reduces the stabilized smoke layer depth and corresponding hot layer temperature.

The influence of soffit height and sill height on the steel member bottom flange time-temperature history is presented in Figure 26(a) and (b), respectively. Figure 26(a) suggests that increasing the height of the base of the soffit will generally bring down the steel member temperature. This is easy to understand, as the increased height corresponds to a reduced 'down-stand barrier' depth, which lowers both the accumulated smoke layer depth and corresponding temperature. Figure 26(b) implies that the sill height has very limited influence on the steel member time-temperature histories, unless this value reaches to 1.5 m. Further to the algorithm in the FIRM zone model which considers the net height of the opening, the vent flow regimes and pressure difference for the neutral plane also depend upon this parameter. The full details of this calculation can be found in Janssens[25].

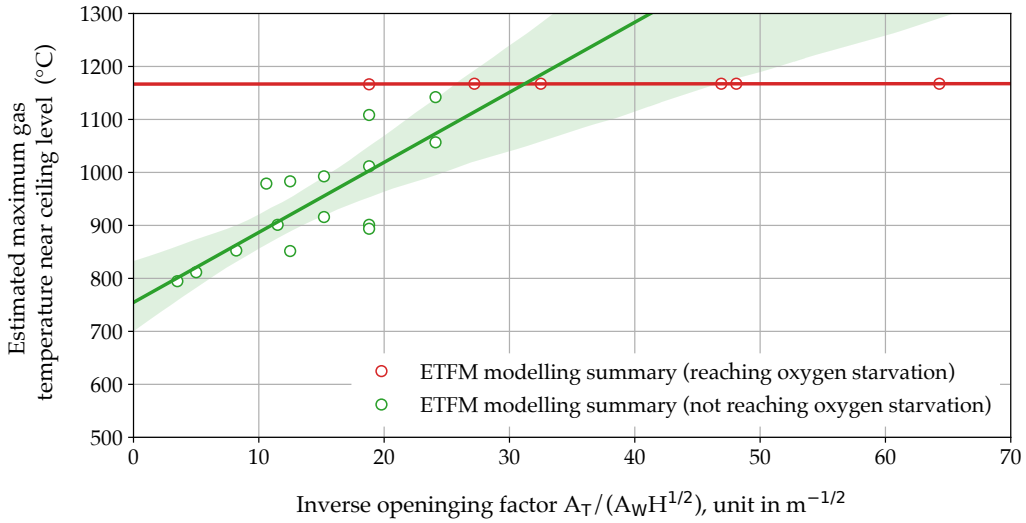

Figure 27. ETFM framework modelling summary of the parametric studies, data based on Figure 25 and Figure 26, in terms of inverse opening factors vs. estimated maximum gas temperatures near ceiling level (the translucent band describes a bootstrap confidence interval of the estimated regression line according to the available data sampling points).

Figure 27 is a summary of the ETFM framework modelling results presented in Figure 25 and Figure 26, in terms of the estimated maximum gas temperatures near ceiling level against the relevant inverse opening factors. This maximum temperature is estimated through dividing the relevant maximum steel member bottom flange temperature by 0.95. This relationship is a rough procedure for estimating the unprotected steel member bottom flange temperature once the surrounding gas temperature is known, as suggested by a HERA report[69]. Unlike the ambiguity of the relationship between the compartment inverse opening factor and the measured maximum gas temperature near the ceiling level (when the compartment inverse opening factor is less than 10 $m^{-1/2}$, experimental review work shown in Figure 4), the green regression line in Figure 27 suggests that the maximum travelling fire temperatures near the ceiling level in the model scale directly with the increasing inverse opening factors. Once the inverse opening factors are large enough, maximum temperature is capped at around 1167°C due to the fact that the ETFM framework fire assumes a single ventilation-controlled situation limited by the air

inflow, i.e. $(\dot{m}_a)_{max} = 0.52A_v\sqrt{H_v}$. In reality the maximum temperatures will eventually decrease again as the inverse opening factors become larger, as suggested from the review of large-scale travelling fire experiments presented in Figure 4. Furthermore, by coincidence Figure 27 suggests that the same value of inverse opening factor (30 $m^{-1/2}$) divides the fuel-controlled regime and ventilation-controlled regime, matching that suggested by Figure 4.

5 Discussion

The ETFM framework was developed for providing a more realistic tool for structural fire design of in large compartments and its application has been demonstrated here with respect to scenarios based on the Veselí travelling fire test. There are several inevitable limitations in the model. Firstly, it is essentially a 1D trajectory-based travelling fire model, which is currently strictly only applicable to floor plans with a core, or rectangular floorplan shape. Secondly, the applicability of Hasemi's localized fire model may be queried, as it is only strictly valid for fire diameters is less than 10m, and rate of heat release less than 50MW[47], though these are very large fire sizes for typical compartments. Also, the FIRM zone model is applicable for the ventilations with vertical openings through the walls, which excludes scenarios such as basement fires, and external winds are not considered[25].

Considering the detailed comparisons with the Veselí test data there are further simplifications: 1) in the model's assumption of a prescribed uniform fire spread rate, though this restriction could easily be relaxed in model; 2) there are large discrepancies in the cooling phase of the fire, with the model over-predicting the temperature decay; this discrepancy is quite problematic, as it will be compounded via the subsequent structural response analysis; 3) uniform smoke layer assumption in the ETFM framework might well be overly conservative for the structural elements in the distant far field, a zone model limitation; 4) though a good comparison in terms of the maximum steel temperatures and the relative timing of different steel member time-temperature histories along the travelling fire trajectory, it is worth noting that Veselí Travelling Fire Test represents a scenario near the transition between "fuel-controlled" and "ventilation-controlled" regimes, while much more complex behaviour might be expected in other some other fire conditions.

6 Conclusions

The full version of the ETFM framework with relevant design instructions, which can be readily used by structural fire engineers, is presented. The ease of using the ETFM framework with a reliable computational tool SIFBuilder, is also demonstrated. It is maintained that the inherent energy balance and mass balance from the FIRM zone model enable the ETFM framework to provide useful and practical insights on the thermal response with various parameters under more realistic fire scenarios (i.e. travelling fires) for performance-based structural fire design.

A number of full-scale natural fire tests in the large compartments, where a clear travelling fire development had been identified or targeted, are reviewed in this paper (Figure 4). Investigation of the relationship between the inverse opening factor $A_T/(A_w H^{1/2})$ and the maximum average gas-phase temperature $T_{g,max}$ near ceiling level suggests that results vary from classical observations in smaller compartments[29]. Through comparing with the conventional regression curve for this relationship in small size compartments (< 150 m^3), it is found that the dependence of the relationship may be weaker for larger compartments, especially for the cases under the fuel-controlled regime. Further, the regime 'division number' apparently shifts from around 10 $m^{-1/2}$ for small compartments to about 30 $m^{-1/2}$ for larger compartments, which is noted from the experimental review and has been observed in small-scale tests[29], and also seems to be supported by model analysis with the ETFM framework (see Figure 27).

Application of the ETFM framework to a real building, i.e. the Veselí Travelling Fire Test building,

representing such a travelling fire scenario, confirms the capability of the ETFM framework in reproducing the maximum steel temperatures and relative timing of different steel member time-temperature histories along the travelling fire trajectory. These capabilities are arguably the most important elements for structural fire design under travelling fires. It is found that the fire spread rate and fuel load density are roughly equally determinative factors on the resultant maximum steel beam temperatures, while the latter value is higher than 800°C for the Veselí Test Building case. However, such 'equivalent influence' diminishes when the travelling fire scenarios move into regimes resulting in lower resultant maximum temperatures, below 800°C. This implies that the fuel load density has a slightly stronger impact than fire spread rate under such fire scenario combinations.

It has been quantitatively demonstrated that the total heat loss fraction (e.g. through ceiling and wall linings) and the inverse opening factors are two important design parameters for travelling fires, which should be carefully selected for the design scenarios. For example, choosing a small inverse opening factor (i.e. large openings compared with the entire compartment) for the design solution, would yield lower maximum steel member temperatures. Non-uniform fire spread rate, and the cooling stage temperatures are identified as avenues for further work.

7 Acknowledgements

The authors would like to express their sincere thanks to those who provided access to relevant fire test data: Johan Sjöström for the TRAFIR-RISE Fire Test, David Rush for the Tisova Fire Test, and Juan P. Hidalgo for the Malveira Fire Test, for the review work of this paper. František Wald, Angus Law, and Juan P. Hidalgo are gratefully acknowledged for their precious suggestions and discussions during the development of this work. We would also like to thank Zhuojun Nan for her assistance in performing the preliminary parametric studies. At last, the authors acknowledge the support from the TRAFIR project, funding from the Research Fund for Coal and Steel (grant N°754198). Partners are ArcelorMittal Belval & Differdange from Luxembourg, University of Liège, University of Edinburgh, RISE from Sweden, and University of Ulster.

8 References

[1] American Society for Testing and Materials. (2016). *Standard Test Methods for Fire Tests of Building Construction and Materials, ASTM E119.*, West Conshohocken, PA.

[2] Hasemi, Y., Yokobayashi, Y., Wakamatsu, T., and Ptchelintsev, A. V. (1996). Modelling of heating mechanism and thermal response of structural components exposed to localised fires, in: *Thirteenth Meeting of the UJNR Planel on Fire Research and Safety*. p. 237–247.

[3] Usmani, A.S., Chung, Y.C., and Torero, J.L. (2003). How did the WTC towers collapse: A new theory, *Fire Safety Journal*, 38(6), pp. 501–533.

[4] Gann, R.G., Hamins, A., McGrattan, K., Nelson, H.E., Ohlemiller, T.J., Prasad, K.R., and Pitts, W.M. (2013). Reconstruction of the fires and thermal environment in World Trade Center buildings 1, 2, and 7, *Fire Technology*, 49, pp. 679–707.

[5] Nelson, H.E. (1989). *An Engineering View of the Fire of May 4, 1988 in the First Interstate Bank Building, Los Angeles, California (NIST IR 89-4061)*, Gaithersburg, National Institute of Standards and Technology (NIST).

[6] Fletcher, I., Borg, A., Hitchen, N., and Welch, S. (2006). Performance of concrete in fire: A review of the state of the art, with a case study of the Windsor Tower fire, in: *4th International Workshop in Structures in Fire*. Aveiro, Portugal: Universidade de Aveiro, p. 779–790.

[7] Behnam, B. (2018). Fire structural response of the Plasco Building: A preliminary investigation report, *International Journal of Civil Engineering*, pp. 1–18.

[8] Yarlagadda, T., Hajiloo, H., Jiang, L., Green, M., and Usmani, A. (2018). Preliminary modelling of Plasco Tower collapse, *International Journal of High-Rise Buildings*, 7(4), pp. 397–408.

[9] Stern-Gottfried, J., and Rein, G. (2012). Travelling fires for structural design–Part I: Literature review, *Fire Safety Journal*, 54, pp. 74–85.

[10] Dai, X., Welch, S., and Usmani, A. (2017). A critical review of "travelling fire" scenarios for performance-based structural engineering, *Fire Safety Journal*, 91, pp. 568–578.

[11] J., S., Cheng, X.D., M., V., Wickström, U., and T., H. (2011). Travelling Fires for CFD, in: *Fire Safety Science*

- *Proceedings of the 10th International Symposium*. p. 1479–1488.
[12] Horová, K., Jána, T., and Wald, F. (2013). Temperature heterogeneity during travelling fire on experimental building, *Advances in Engineering Software*, 62–63, pp. 119–130.
[13] Cheng, X., Zhou, Y., Yang, H., and Li, K. (2014). Numerical Study on Temperature Distribution of Structural Components Exposed to Travelling Fire, *Procedia Engineering*, 71, pp. 166–172.
[14] Charlier, M., Gamba, A., Dai, X., Welch, S., Vassart, O., and Franssen, J. (2018). CFD analyses used to evaluate the influence of compartment geometry on the possibility of development of a travelling fire, in: *Proceedings of the 10th International Conference on Structures in Fire (SiF 2018)*. FireSERT, Ulster University, Belfast, UK, p. 341–348.
[15] Kallada Janardhan, R., and Hostikka, S. (2019). Predictive computational fluid dynamics simulation of fire spread on wood cribs, *Fire Technology*, 55, pp. 2245–2268.
[16] Dai, X., Welch, S., Rush, D., Charlier, M., and Anderson, J. (2019). Characterising natural fires in large compartments – revisiting an early travelling fire test (BST/FRS 1993) with CFD, in: *15th International Interflam Conference*. London, UK, p. 2111–2122.
[17] Anderson, J., Sjöström, J., Temple, A., Charlier, M., Dai, X., Welch, S., and Rush, D. (2019). FDS simulations and modelling efforts of travelling fires in a large elongated compartment, in: *15th International Interflam Conference*. London, UK, p. 2085–2094.
[18] Clifton, C.G. (1996). *Fire Models for Large Firecells. HERA Report R4-83*, HERA publications, New Zealand.
[19] Rein, G., Zhang, X., Williams, P., Hume, B., Heise, A., Jowsey, A., Lane, B., and Torero, J.L. (2007). Multi-storey fire analysis for high-rise buildings, in: *Proceedings of the 11th International Interflam Conference*. London, UK, p. 605–616.
[20] Stern-Gottfried, J., and Rein, G. (2012). Travelling fires for structural design-Part II: Design methodology, *Fire Safety Journal*, 54, pp. 96–112.
[21] Hopkin, D. (2013). Testing the single zone structural fire design hypothesis, in: *Proceedings of the 13th International Interflam Conference*. London, UK, p. 139–150.
[22] Rackauskaite, E., Hamel, C., Law, A., and Rein, G. (2015). Improved formulation of travelling fires and application to concrete and steel structures, *Structures*, 3, pp. 250–260.
[23] Dai, X., Jiang, L., Maclean, J., Welch, S., and Usmani, A. (2016). A conceptual framework for a design travelling fire for large compartments with fire resistant islands, in: *Proceedings of the 14th International Interflam Conference*. London, UK, p. 1039–1050.
[24] Dai, X., Jiang, L., Maclean, J., Welch, S., and Usmani, A. (2016). Implementation of a new design travelling fire model for global structural analysis, in: *The 9th International Conference on Structures in Fire*. Princeton, USA, p. 959–966.
[25] Janssens, M.L. (2000). *An Introduction to Mathematical Fire Modeling*, Second Edi, CRC Press.
[26] Drysdale, D. (2011). *An Introduction to Fire Dynamics*, Third Edit, Chichester, UK, A John Wiley & Sons, Ltd., Publication.
[27] Thomas, P.H., and Heselden, A.J. (1972). *Fully developed fires in single compartments, CIB Report No 20, Fire Research Note 923*, Borehamwood, England, UK.
[28] Torero, J.L., Majdalani, A.H., Abecassis-Empis, C., and Cowlard, A. (2014). Revisiting the compartment fire, in: *11th International Symposium on Fire Safety Science*. Christchurch, New-Zealand: International Association for Fire Safety Science, p. 28–45.
[29] Majdalani, A.H., Cadena, J.E., Cowlard, A., Munoz, F., and Torero, J.L. (2016). Experimental characterisation of two fully-developed enclosure fire regimes, *Fire Safety Journal*, 79, pp. 10–19.
[30] Maluk, C., Linnan, B., Wong, A., Hidalgo, J.P., Torero, J.L., Abecassis-empis, C., and Cowlard, A. (2017). Energy distribution analysis in full-scale open floor plan enclosure fires, *Fire Safety Journal*, 91, pp. 422–431.
[31] Hidalgo, J.P., Cowlard, A., Abecassis-Empis, C., Maluk, C., Majdalani, A.H., Kahrmann, S., Hilditch, R., Krajcovic, M., and Torero, J.L. (2017). An experimental study of full-scale open floor plan enclosure fires, *Fire Safety Journal*, 89, pp. 22–40.
[32] Kirby, B.R., Wainman, D.E., Tomlinson, L.N., Kay, T.R., and Peacock, B.N. (1994). *Natural Fires in Large Scale Compartments*, British Steel Technical, Fire Research Station Collaborative Project Report, Rotherham, UK.
[33] British Steel plc, and Swinden Technology Centre. (1999). *The Behaviour of Multi-Storey Steel Framed Buildings in Fire (A European Joint Research Programme)*, Rotherham, UK.
[34] Moss, P.J., and Clifton, G.C. (2004). Modelling of the Cardington LBTF steel frame building fire tests, *Fire and Materials*, 28(2–4), pp. 177–198.
[35] Moinuddin, K.A.M., and Thomas, I.R. (2009). An experimental study of fire development in deep enclosures and a new HRR–time–position model for a deep enclosure based on ventilation factor, *Fire and Materials*, 33, pp. 157–185.
[36] Hidalgo, J.P., Cowlard, A., Abecassis-Empis, C., Maluk, C., Majdalani, A.H., Kahrmann, S., Hilditch, R., Krajcovic, M., and Torero, J.L. (2018). *Edinburgh Tall Building Fire Tests [dataset]*, School of Engineering,

University of Edinburgh.
[37] Goode, T. (2018). *Characterisation of the "Malveira Fire Test", Master Thesis*, The University of Queensland.
[38] Hidalgo, J.P., Goode, T., Gupta, V., Cowlard, A., Abecassis-empis, C., Maclean, J., Bartlett, A.I., Maluk, C., Montalvá, J.M., Osorio, A.F., and Torero, J.L. (2019). The Malveira fire test : Full-scale demonstration of fire modes in open-plan compartments, *Fire Safety Journal*, 108, pp. n/a.
[39] Rush, D., and Lange, D. (2017). Towards a fragility assessment of a concrete column exposed to a real fire – Tisova Fire Test, *Engineering Structures*, 150, pp. 537–549.
[40] Gales, J. (2014). Travelling fires and the St. Lawrence Burns project, *Fire Technology*, 50(6), pp. 1535–1543.
[41] Hasemi, Y., and Tokunaga, T. (1984). Flame geometry effects on the buoyant plumes from turbulent diffusion flames, *Fire Science and Technology*, 4, pp. 15–26.
[42] Hasemi, Y., Yokobayashi, Y., Wakamatsu, T., and Ptchelintsev, A. (1995). Fire safety of building components exposed to a localized fire - scope and experiments on ceiling beam system exposed to a localized fire, in: *ASIAFLAM'95, Hong Kong*. Hong Kong.
[43] Pchelintsev, A., Hasemi, Y., Wakamatsu, T., and Yokobayashi, Y. (1997). Experimental and numerical study on the behaviour of a steel beam under ceiling exposed to a localized fire, in: *Fire Safety Science - Proceedings of the 5th International Symposium*. p. 1153–1164.
[44] Wakamatsu, T., Hasemi, Y., and Ptchelintsev, A. V. (1997). Heating mechanism of building components exposed to a localized fire - FDM thermal analysis of a steel beam under ceiling, in: *Proceedings of the 1997 16th International Conference on Offshore Mechanics and Arctic Engineering*. Yokohama, Japan: ASME, p. 51–58.
[45] Kruppa, J., Joyeux, D., and Zhao, B. (2005). Scientific background to the harmonization of structural Eurocodes, *HERON*, 50(4), pp. 219–235.
[46] Commission of the European Community (CEC) (1997b). (1997). *Development of Design Rules for Steel Structures Subjected to Natural Fires in Closed Car Parks*.
[47] CEN, E.S.E. 1991-1-2. (2002). *Eurocode1: Actions on Structures - Part 1-2: General Actions - Actions on Structures Exposed to Fire*, Brussels.
[48] Cadorin, J.-F., and Franssen, J.-M. (2003). A tool to design steel elements submitted to compartment fires—OZone V2. Part 1: pre- and post-flashover compartment fire model, *Fire Safety Journal*, 38(5), pp. 395–427.
[49] Cadorin, J.-F., Pintea, D., Dotreppe, J.-C., and Franssen, J.-M. (2003). A tool to design steel elements submitted to compartment fires—OZone V2. Part 2: Methodology and application, *Fire Safety Journal*, 38(5), pp. 429–451.
[50] Peacock, R.D., Mcgrattan, K.B., Forney, G.P., and Reneke, P.A. (2017). *CFAST – Consolidated Fire and Smoke Transport (Version 7) Volume 1 : Technical Reference Guide*, National Institute of Standards and Technology.
[51] American Society for Testing and Materials. (2004). *ASTM E1355-04, Standard Guide for Evaluating the Predictive Capabilities of Deterministic Fire Models*, West Conshohocken, Pennsylvania.
[52] Kumar, S., Chitty, R., and Welch, S. (2003). Development and validation of integrated fire modelling methodology for smoke ventilation design and hazard assessment in large buildings, in: *Proceedings of the 4th International Seminar on Fire & Explosion Hazards*. p. 629–641.
[53] Thomas, P.H., Hinkley, P.L., and Theobald, C.R. (1963). *Investigations into the Flow of Hot Gases in Roof Venting*, BRE Archive.
[54] Zukoski, E.E., Kubota, T., and Cetegen, B. (1981). Entrainment in fire plumes, *Fire Safety Journal*, 3(3), pp. 107–121.
[55] Franssen, J., Gamba, A., and Charlier, M. (2019). Toward a standardized uniformly distributed cellulosic fire load, in: *IFireSS 2019 – 3rd International Fire Safety Symposium*. Ottawa, Ontario, Canada, p. 1–8.
[56] Babrauskas, V. (1998). Glass breakage in fires, *The Fire Place, Washington Chapter IAAI Newsletter*, pp. 15–17.
[57] McKenna, F.T. (1997). *Object-Oriented Finite Element Programming: Frameworks for Analysis, Algorithms and Parallel Computing*, PhD Thesis, the University of California.
[58] Dai, X., Jiang, Y., Jiang, L., Welch, S., and Usmani, A.S. (2017). Implementation of fire models in OpenSees, in: *Proceedings of the 1st European Conference on OpenSees*. Porto, Portugal: Faculty of Engineering, University of Porto, p. 47–50.
[59] Dai, X. (2017). *An extended travelling fire method framework with an OpenSees-based integrated tool SIFBuilder*, PhD Thesis, The University of Edinburgh.
[60] Jiang, L., Dai, X., Usmani, A., and Kamath, P. (2015). OpenSees-based integrated tool for modelling structures in fire, in: *The First International Conference on Structural Safety under Fire & Blast, Glasgow, Scotland, UK*. Glasgow, Scotland, UK: The First International Conference on Structural Safety under Fire & Blast, p. 461–468.
[61] Jiang, L., and Usmani, A. (2018). Towards scenario fires – modelling structural response to fire using an integrated computational tool, *Advances in Structural Engineering*, 21(13), pp. 2056–2067.
[62] Simões da Silva et al., L. (2014). *Design of Composite Joints for Improved Fire Robustness, RFCS Compfire project-final report (RFSR-CT-2009-00021)*, Luxembourg.
[63] Wald, F., Jána, T., and Horová, K. (2011). *Design of Joints to Composite Columns for Improved Fire*

Robustness: To Demonstration Fire Tests, Czech Technical University in Prague.
[64] Horová, K. (2015). *Modelling of Fire Spread in Structural Fire Engineering*, PhD Thesis, Czech Technical University in Prague.
[65] Karlsson, B., and Quintiere, J.G. (1999). *Enclosure Fire Dynamics*, 1st Edi, CRC Press.
[66] Jiang, Y. (2012). *Development and Application of a Thermal Analysis Framework in OpenSees for Structures in fire*, PhD Thesis, the University of Edinburgh.
[67] Welch, S., Jowsey, A., Deeny, S., Morgan, R., and Torero, J.L. (2007). BRE large compartment fire tests-Characterising post-flashover fires for model validation, *Fire Safety Journal*, 42(8), pp. 548–567.
[68] Torero, J.L. (2013). Scaling-Up fire, *Proceedings of the Combustion Institute*, 34, pp. 99–124.
[69] HERA. (2006). *Steel Structures Seminar: Earthquake, Wind and Fire, HERA Report R4-139*, Manukau City, New Zealand, New Zealand Heavy Engineering Research Association.